Research Article

Mathematical study on two-fluid model for flow of K–L fluid in a stenosed artery with porous wall

R. Ponalagusamy[1] · Ramakrishna Manchi[1]

Abstract

The present communication presents a theoretical study of blood flow through a stenotic artery with a porous wall comprising Brinkman and Darcy layers. The governing equations describing the flow subjected to the boundary conditions have been solved analytically under the low Reynolds number and mild stenosis assumptions. Some special cases of the problem are also presented mathematically. The significant effects of the rheology of blood and porous wall of the artery on physiological flow quantities have been investigated. The results reveal that the wall shear stress at the stenotic throat increases dramatically for the thinner porous wall (i.e. smaller values of the Brinkman and Darcy regions) and the rate of increase is found to be 18.46% while it decreases for the thicker porous wall (i.e. higher values of the Brinkman and Darcy regions) and the rate of decrease is found to be 10.21%. Further, the streamline pattern in the stenotic region has been plotted and discussed.

Keywords Arterial stenosis · K–L model fluid · Porous wall · Plug flow · Transition Brinkman layer · Darcy number

1 Introduction

Arteries are the blood vessels that transport blood from the heart to all parts of the body (lungs, tissues, brain etc.). In many cases, some obstructions occur in the arteries during the blood flow, and one of them is the deposition of plaques on the arterial walls, narrowing the area of the flow region and leading to a disease called atherosclerosis or stenosis. Over a period, stenosis solidifies and constricts the blood vessels, limiting the oxygenated blood supply to the organs and other parts of the body which leads to severe complications, including heart attack, stroke, or even death [6].

To understand the influence of constriction in the lumen of a blood vessel, many research workers [8, 17, 31] have studied the blood flow through the constricted arteries by supposing it as a Newtonian viscous fluid. Mekheimer and Kot [18] presented a particle-fluid suspension model for blood flow through a catheterized curved artery with constriction. The effect of a catheter on entropy generation in two-phase blood flow is analytically studied by Mekheimer et al. [19]. Elnaqeeb et al. [11] examined the influence of *Cu* nanoparticles on the flow of blood, assuming the rheology of blood as Newtonian fluid in a catheterized arterial stenosis with a clot. But it is well recognized that as it flows through small-diameter vessels at low shear rates, blood exhibits non-Newtonian fluid behavior [9, 15, 30]. The papers [25, 28] include a brief sample of the scientific work on non-Newtonian effects on blood flow by considering blood as a Casson model fluid, in view of the non-Newtonian nature of blood. Akbar et al. [1] investigated the Reiner–Rivlin model fluid for blood flow in a tapered mild stenotic artery. In addition, Bugliarello, Sevilla [7] and Cokelet [10] have experimentally confirmed that there is a peripheral plasma layer (Newtonian viscous fluid) near the vessel wall and a central area of suspension of all

✉ Ramakrishna Manchi, manchinitt2017@gmail.com; R. Ponalagusamy, rpalagu@nitt.edu | ¹Department of Mathematics, National Institute of Technology, Tiruchirappalli 620015, Tamil Nadu, India.

erythrocytes as a non-Newtonian fluid when blood passes through the small blood vessels. Several authors [13, 20, 23] have examined the two-layered model of blood flow in a stenosed artery in which the central core region consisting of Casson fluid and the peripheral layer containing the Newtonian fluid.

In the studies as mentioned above, the blood flow through the blood vessels is considered as single or double-layered, and the vessel walls are treated as rigid. While the blood vessel walls are structurally composed primarily of three layers: tunica intima, tunica media, and tunica externa. The porous medium is a substance composed of a rigid frame of pores that are intertwined. The flow through porous media was explored by Whitaker [29] using Darcy's law. Goharzadeh et al. [12] have experimentally examined the existence and thickness of the transition layer at a fluid porous interface. A three-layer structure in which a Newtonian fluid is overlying a transition porous layer, which overlays a layer of the porous region of Darcy, has been studied by Hill and Straughan [14], and they have discussed the instability of Poiseuille flow. Boodoo et al. [5] have proposed a two-fluid mathematical model for blood flow in a uniform tube such that the wall of the tube is assumed to be porous and consisting of a thin transition Brinkman layer followed by a Darcy region. In their model, the central core region comprises a micropolar fluid, and the peripheral plasma layer, Brinkman, and Darcy regions are filled with Newtonian fluid. The study shows that the fluid velocity in the core region and plasma layer reduces with the increase of hydraulic resistivity, and the smaller values of permeability increase the flow resistance in the porous region that causes an overall slower velocity of both the fluids in the core and plasma. Sharma and Yadav [24] have discussed a Casson–Newtonian fluid model for blood flow in a stenotic artery with the porous wall which comprises a Brinkman layer (tunica intima) surrounding a Darcy region. They concluded that as the yield stress increases, the Casson fluid velocity reduces, and the flow rate in the stenotic region has a symmetric profile for the stenosis shape parameter $n = 2$, but for other values of n, it is asymmetric.

The Kuang–Luo (K–L) model fluid, which is an improvement of the Casson model, has been proposed by Luo and Kuang [16]. It provides a better depiction of the non-Newtonian character of blood since it encompasses three parameters, such as yield stress, plasma viscosity, and other chemical variables, whereas only viscosity and yield stress are considered in the Casson model. In describing the shear-thinning behavior of blood within an extensive shear rate, this model is more effective [16]. The constitutive blood parameters were experimentally explored in various blood rheological equations by Zhang and Kuang [32]. The investigation revealed that Bi-exponent, Quemada, and K–L models are in good agreement with the hemorheological features of canine and human blood, and the K–L model can be used well in hemorheology and hemodynamics. Several authors [2, 3, 26] have been introduced mathematical models to illustrate the effect of stenosis on blood flow characteristics treating blood as K–L model fluid.

With this motivation, an attempt is made to study a two-fluid mathematical model for blood flow in a constricted artery consisting of a core region of suspension of all the erythrocytes supposed to be a K–L fluid and a peripheral layer of plasma as a Newtonian fluid. The arterial wall segment is assumed to be porous and comprising two-layers, namely Brinkman and Darcy. The layout of the paper is as follows. Section 2 deals with the formulation of the problem in which the equations of motion for all the four regions using K–L and Newtonian constitutive equations and the non-dimensionalization procedure are presented. The resulting differential equations are solved with the appropriate boundary conditions, and the analytic expressions for the physiologically significant flow quantities such as velocity profiles in all the regions, plug-core radius, flow flux, wall shear stress, and resistive impedance are obtained in Sect. 3. Some special cases, which are the limiting cases of the present model, are presented in Sect. 4. The impact of several physical parameters on the blood flow characteristics is analyzed in Sect. 5. The outcomes are summarized, and the significance of the presence of the peripheral plasma layer and the porous wall is indicated in the concluding Sect. 6.

2 Modeling and formulation

Consider one dimensional, steady, laminar, fully developed, and an axially symmetric flow of incompressible viscous fluid (blood) through the stenosed artery whose porous wall is composed of two layers, namely Brinkman and Darcy. We assume that the rheology of blood in the core region is characterized by the K–L fluid and a peripheral layer of plasma, porous wall as a Newtonian fluid. A cylindrical polar coordinate system $(\bar{r}, \bar{\theta}, \bar{z})$ whose origin is located on the vessel (constricted artery) axis is taken to examine the flow of blood. The geometry of the stenotic arterial segment (see Fig. 1) in dimensional form is written mathematically as

$$\frac{\overline{R}(\bar{z})}{\overline{R}_0} = \begin{cases} 1 - \overline{\chi}\{\overline{L}_0^{m-1}(\bar{z} - \overline{d}) - (\bar{z} - \overline{d})^m\}, & \overline{d} \le \bar{z} < \overline{d} + \overline{L}_0; \\ 1, & otherwise \end{cases}$$

(1)
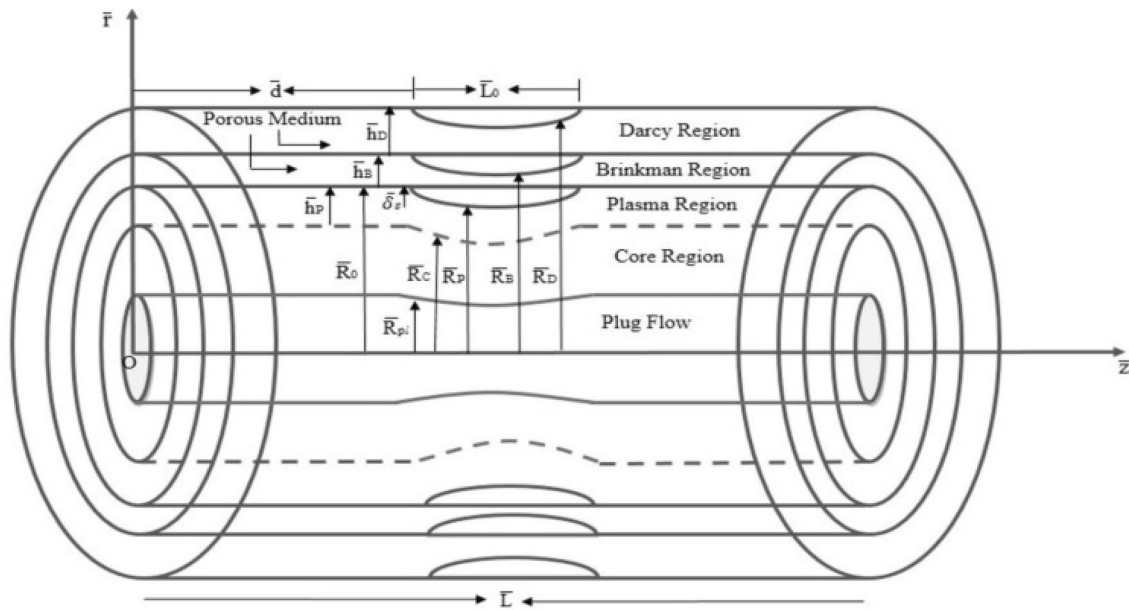
Fig. 1 Schematic diagram of a stenosed artery with different regions

where $\overline{\chi} = \dfrac{\overline{\delta}_s}{\overline{R}_0 \overline{L}_0^{-m}} \left(\dfrac{m^{m/(m-1)}}{m-1} \right)$, $\overline{R}(\overline{z})$, $\overline{R}_0$ are the radius of the duct with and without stenosis, respectively, $\overline{R}_{pl}$ is the plug core radius, $\overline{d}$ is the location of the constriction, $\overline{L}_0$ indicates its length, $m (\geq 2)$ is the stenotic shape parameter, $\overline{\delta}_s$ is the maximum stenotic height occurs at $\overline{z} = \overline{d} + \dfrac{\overline{L}_0}{m^{1/(m-1)}}$, such that $\dfrac{\overline{\delta}_s}{\overline{R}_0} << 1$. We denote $\overline{R}_C, \overline{R}_P, \overline{R}_B$ and $\overline{R}_D$ be the radius of the duct in the stenotic region for core, plasma, Brinkman and Darcy regions, respectively. Let $\overline{h}_P, \overline{h}_B$ and $\overline{h}_D$ represent the thickness of the plasma, Brinkman and Darcy layers, respectively such that $\overline{h}_B = \overline{h}_D/9$ [27].

Let us assume $\overline{P}_C, \overline{P}_P, \overline{P}_B$ and $\overline{P}_D$ be the pressures in the four regions, respectively. As the flow is one dimensional (axial direction) and axially symmetric, the velocity vector is given by $\overline{\mathbf{V}} = (0, 0, \overline{w}_i)$, where $\overline{w}_i$ is the axial velocity in the respective region ($i = C, P, B,$ and D). Hence the basic momentum equations for the four regions can be written as:

Region I: Core region (K–L fluid)

$$-\frac{\partial \overline{P}_C}{\partial \overline{z}} + \frac{1}{\overline{r}} \frac{\partial}{\partial \overline{r}} \left(\overline{r} \, \overline{\tau}_{\overline{r}\overline{z}} \right) = 0, \tag{2}$$

where the shear stress $\overline{\tau}_{\overline{r}\overline{z}}$, for K–L fluid, is given by [16]

$$\overline{\tau}_{\overline{r}\overline{z}} = \overline{\tau}_0 + \overline{\sigma}_1 \sqrt{\dot{\overline{\gamma}}} + \overline{\sigma}_2 \dot{\overline{\gamma}}, \quad \overline{\tau}_{\overline{r}\overline{z}} > \overline{\tau}_0 \tag{3}$$

$$\dot{\overline{\gamma}} = 0, \overline{\tau}_{\overline{r}\overline{z}} \leq \overline{\tau}_0 \tag{4}$$

Region II: Plasma region (Newtonian fluid)

$$-\frac{\partial \overline{P}_P}{\partial \overline{z}} + \frac{\overline{\mu}}{\overline{r}} \frac{\partial}{\partial \overline{r}} \left(\overline{r} \frac{\partial \overline{w}_P}{\partial \overline{r}} \right) = 0 \tag{5}$$

Region III: Brinkman porous region (Newtonian fluid)

$$-\frac{\partial \overline{P}_B}{\partial \overline{z}} + \frac{\overline{\mu}_e}{\overline{r}} \frac{\partial}{\partial \overline{r}} \left(\overline{r} \frac{\partial \overline{w}_B}{\partial \overline{r}} \right) - \frac{\overline{\mu}}{k} \overline{w}_B = 0 \tag{6}$$

Region IV: Darcy porous region (Newtonian fluid)

$$-\frac{\partial \overline{P}_D}{\partial \overline{z}} - \frac{\overline{\mu}}{k} \overline{w}_D = 0, \tag{7}$$

where $\dot{\overline{\gamma}}$ is the shear rate, the three parameters $\overline{\tau}_0, \overline{\sigma}_1, \overline{\sigma}_2$ are functions of hematocrit (volume fraction of red blood cells), plasma viscosity, and other chemical variables, $\overline{\mu}_e$ is the effective viscosity of transition (Brinkman) layer and $\overline{k}$ is the permeability constant.

We introduce the following dimensionless variables:

$$z = \frac{\bar{z}}{\bar{R}_0}, \quad r = \frac{\bar{r}}{\bar{R}_0},$$

$$d = \frac{\bar{d}}{\bar{R}_0}, \quad L_0 = \frac{\bar{L}_0}{\bar{R}_0}, \quad \delta_s = \frac{\bar{\delta}_s}{\bar{R}_0},$$

$$R(z) = \frac{\bar{R}(\bar{z})}{\bar{R}_0},$$

$$R_i(z) = \frac{\bar{R}_i(\bar{z})}{\bar{R}_0}, \quad w_i = \frac{\bar{w}_i}{\bar{w}_0}, \quad P_i = \frac{\bar{R}_0 \bar{P}_i}{\bar{w}_0 \bar{\mu}},$$

$$\theta_1 = \frac{\bar{\sigma}_1}{\bar{\mu}} \left(\frac{\bar{R}_0}{\bar{u}_0} \right)^{1/2}, \quad \theta_2 = \frac{\bar{\sigma}_2}{\bar{\mu}}, \tag{8}$$

$$\lambda_e = \frac{\bar{\mu}_e}{\bar{\mu}}, \quad Da = \frac{\bar{k}}{\bar{R}_0^2}, \quad \tau_{rz} = \frac{\bar{R}_0 \bar{\tau}_{\bar{r}\bar{z}}}{\bar{w}_0 \bar{\mu}},$$

$$\tau_0 = \frac{\bar{R}_0 \bar{\tau}_0}{\bar{w}_0 \bar{\mu}}, \quad Re = \frac{\bar{\rho} \bar{R}_0 \bar{w}_0}{\bar{\mu}},$$

where $\bar{\mu}$ is the Newtonian fluid viscosity, θ_1 and θ_2 are the non-dimensional K–L fluid parameters, Da is the Darcy number, λ_e is the non-dimensional effective viscosity and Re is the Reynolds number. Equations (2)–(7) can be transformed to dimensionless form by employing the above non-dimensional variables:

Region I: Core region

$$-\frac{\partial P_C}{dz} + \frac{1}{r} \frac{\partial}{\partial r} \left(r \, \tau_{rz} \right) = 0 \tag{9}$$

where

$$\tau_{rz} = \tau_0 + \theta_1 \sqrt{-\frac{\partial w_C}{\partial r}} - \theta_2 \frac{\partial w_C}{\partial r}, \quad \tau_{rz} > \tau_0 \tag{10}$$

$$-\frac{\partial u_C}{\partial r} = 0, \tau_{rz} \leq \tau_0 \tag{11}$$

It is emphasized from the Eqs. (10) and (11) that the velocity gradients vanish in the flow region where the shear stress (τ_{rz}) is less than the yield stress (τ_0), which in turn indicates that the plug flow occurs whenever $\tau_{rz} \leq \tau_0$. However, normal flow occurs whenever $\tau_{rz} > \tau_0$ (i.e. the shear stress is greater than the threshold stress).

Region II: Plasma region

$$-\frac{\partial P_P}{\partial z} + \frac{1}{r} \frac{\partial}{\partial r} \left(r \frac{\partial w_P}{\partial r} \right) = 0 \tag{12}$$

Region III: Brinkman porous region

$$-\frac{\partial P_B}{\partial z} + \frac{\lambda_e}{r} \frac{\partial}{\partial r} \left(r \frac{\partial w_B}{\partial r} \right) - \frac{1}{Da} w_B = 0 \tag{13}$$

Region IV: Darcy porous region

$$-\frac{\partial P_D}{\partial z} - \frac{1}{Da} w_D = 0 \tag{14}$$

The boundary conditions are

$$(i) \; \tau_{rz} \text{ is finite at } r = 0 \tag{15}$$

$$(ii) -\frac{\partial w_P}{\partial r} = \tau_0$$
$$+ \theta_1 \left(-\frac{\partial w_C}{\partial r} \right)^{1/2} + \theta_2 \left(-\frac{\partial w_C}{\partial r} \right) \text{ at } r = R_C(z) \tag{16}$$

$$(iii) \; w_C = w_P \text{ at } r = R_C(z) \tag{17}$$

$$(iv) \; w_P = w_B \text{ at } r = R_P(z) \tag{18}$$

$$(v) \; \frac{1}{\phi} \left(\frac{\partial w_B}{\partial r} \right) - \left(\frac{\partial w_P}{\partial r} \right) = \frac{\beta}{\sqrt{Da}} w_B \text{ at } r = R_P(z) \tag{19}$$

where ϕ is the porosity of the medium and β is the parameter of the stress jump [21].

$$(vi) \; \frac{\partial w_B}{\partial r} = \frac{\alpha}{\sqrt{Da}} (w_B - w_D) \text{ at } r = R_B(z) \tag{20}$$

where α is the parameter of the Darcy slip [4].

$$(vii) \; \frac{\partial w_C}{\partial r} = 0 \text{ at } r = R_{pl}(z) \tag{21}$$

The dimensionless form of the wall geometry is given by

$$R(z) = \begin{cases} 1 - \chi \left[L_0^{m-1}(z-d) - (z-d)^m \right], & d \leq z < d + L_0; \\ 1, & \text{otherwise} \end{cases} \tag{22}$$

where $\chi = \frac{\delta_s}{L_0^m} \left(\frac{m^{m/(m-1)}}{m-1} \right)$.

3 Solution

Suppose the pressure gradient in all the four regions are equal.

$$-\frac{\partial P_C}{\partial z} = -\frac{\partial P_P}{\partial z} = -\frac{\partial P_B}{\partial z} = -\frac{\partial P_D}{\partial z} = P_g(z) \tag{23}$$

Substituting Eq. (23) in Eq. (9) and integrating, we get

$$\tau_{rz} = -\frac{rP_g}{2} + \frac{A_1}{r} \tag{24}$$

Using the boundary condition (15), Eq. (24) becomes

$$\tau_{rz} = -\frac{rP_g}{2} \tag{25}$$

The solutions of Eqs. (10)–(14) can be obtained as

$$
w_C = \left(\frac{2\tau_0\theta_2 - \theta_1^2}{2\theta_2^2} \right) r \\
- \frac{P_g r^2}{4\theta_2} + \frac{\theta_1}{6P_g\theta_2^3}\left(\theta_1^2 - 4\tau_0\theta_2 + 2P_g\theta_2 r\right)^{3/2} + A_2 \tag{26}
$$

$$w_P = -\frac{P_g r^2}{4} + A_3 \ln(r) + A_4 \tag{27}$$

$$w_B = A_5 I_0(\xi r) + A_6 K_0(\xi r) + P_g Da \tag{28}$$

$$w_D = P_g Da \tag{29}$$

where $\xi = \dfrac{1}{\sqrt{\lambda_e Da}}$, I_0 and K_0 are modified Bessel functions of first and second kind, respectively and A_2, A_3, A_4, A_5 and A_6 are arbitrary constants to be determined.

The velocity in the plug core region is obtained by

$$
w_{pl} = \left(\frac{2\tau_0\theta_2 - \theta_1^2}{2\theta_2^2} \right) R_{pl} \\
- \frac{P_g R_{pl}^2}{4\theta_2} + \frac{\theta_1}{6P_g\theta_2^3}\left(\theta_1^2 - 4\tau_0\theta_2 + 2P_g\theta_2 R_{pl}\right)^{3/2} + A_2 \tag{30}
$$

Applying boundary condition (16), we get

$$A_3 = 0 \tag{31}$$

By applying boundary conditions (17)–(20), one can obtain

$$
A_2 - A_4 = -\frac{\theta_1}{6P_g\theta_2^3}\left(\theta_1^2 - 4\tau_0\theta_2 + 2P_g\theta_2 R_C\right)^{3/2} \\
- \frac{1}{2\theta_2^2}\left(2\tau_0\theta_2 - \theta_1^2\right)R_C + \frac{P_g}{4\theta_2}(1 - \theta_2)R_C^2 \tag{32}
$$

$$A_4 - I_0(\xi R_P)A_5 - K_0(\xi R_P)A_6 = \frac{P_g}{4}(R_P^2 + 4Da) \tag{33}$$

$$
\left[\phi\beta I_0(\xi R_P) - \xi\sqrt{Da}I_1(\xi R_P)\right]A_5 \\
+ \left[\xi\sqrt{Da}K_1(\xi R_P) + \phi\beta K_0(\xi R_P)\right]A_6 \\
= \frac{\phi P_0}{2}\left(R_P\sqrt{Da} - 2\beta Da\right) \tag{34}
$$

$$
\left[\alpha I_0(\xi R_B) - \xi\sqrt{Da}I_1(\xi R_B)\right]A_5 \\
+ \left[\alpha K_0(\xi R_B) + \xi\sqrt{Da}K_1(\xi R_B)\right]A_6 = 0 \tag{35}
$$

where A_2, A_4, A_5 and A_6 are arbitrary constants which can be found out by solving the Eqs. (32)–(35) using MATLAB software, and are given in "Appendix".

Applying boundary condition (21), we can obtain the expression for plug core radius

$$R_{pl} = \frac{2\tau_0}{P_g} \tag{36}$$

The flow rate through the plug core region Q_{pl} is defined as

$$Q_{pl} = \int_0^{R_{pl}} r\, u_{pl}\, dr \tag{37}$$

which, on substituting Eq. (30), gives

$$
Q_{pl} = \frac{\theta_1 R_{pl}^2}{12P_g\theta_2^3}\left(\theta_1^2 - 4\tau_0\theta_2 + 2P_g R_{pl}\theta_2\right)^{3/2} \\
+ \frac{1}{4\theta_2^2}\left(2\tau_0\theta_2 - \theta_1^2\right)R_{pl}^3 \\
- \frac{P_g R_{pl}^4}{8\theta_2} + \frac{A_2 R_{pl}^2}{2} \tag{38}
$$

Similarly, the flux through the core, plasma, Brinkman and Darcy regions may be expressed as

$$
Q_C = \frac{1}{6\theta_2^2}\left(2\tau_0\theta_2 - \theta_1^2\right)\left(R_C^3 - R_{pl}^3\right) + \frac{P_g}{16\theta_2}\left(R_{pl}^4 - R_C^4\right) \\
+ \frac{A_2}{2}\left(R_C^2 - R_{pl}^2\right) \\
+ \frac{\theta_1}{210P_g^3\theta_2^5}\left(\theta_1^2 - 4\tau_0\theta_2 + 2P_g\theta_2 R_C\right)^{5/2} \\
\left(-\theta_1^2 + 4\tau_0\theta_2 + 5P_g\theta_2 R_C\right) \\
- \frac{\theta_1}{210P_g^3\theta_2^5}\left(\theta_1^2 - 4\tau_0\theta_2 + 2P_g\theta_2 R_{pl}\right)^{5/2} \\
\left(-\theta_1^2 + 4\tau_0\theta_2 + 5P_g\theta_2 R_{pl}\right) \tag{39}
$$

$$Q_P = \frac{P_g}{16}\left(R_C^4 - R_P^4\right) + \frac{A_4}{2}\left(R_P^2 - R_C^2\right) \tag{40}$$

$$Q_B = \frac{A_5}{\xi}\left[R_B I_1(\xi R_B) - R_P I_1(\xi R_P)\right]$$
$$- \frac{A_6}{\xi}\left[R_B K_1(\xi R_B) - R_P K_1(\xi R_P)\right] \tag{41}$$
$$+ \frac{P_g Da}{2}\left(R_B^2 - R_P^2\right)$$

$$Q_D = \frac{P_g Da}{2}\left(R_D^2 - R_B^2\right) \tag{42}$$

The total volumetric flux is calculated as

$$Q = Q_{pl} + Q_C + Q_P + Q_B + Q_D \tag{43}$$

Substituting Eqs. (38)–(42) in Eq. (43), the expression for flux can be written as

$$Q = \frac{1}{12\theta_2^2}\left(2\tau_0\theta_2 - \theta_1^2\right)\left(R_{pl}^3 + 2R_C^3\right)$$
$$- \frac{P_g}{16\theta_2}\left(R_{pl}^4 + (1-\theta_2)R_C^4 + \theta_2 R_P^4\right)$$
$$+ \frac{P_g Da}{2}\left(R_D^2 - R_P^2\right) + \frac{A_4}{2}\left(R_P^2 - R_C^2\right)$$
$$+ \frac{A_5}{\xi}\left[R_B I_1(\xi R_B) - R_P I_1(\xi R_P)\right]$$
$$- \frac{A_6}{\xi}\left[R_B K_1(\xi R_B) - R_P K_1(\xi R_P)\right]$$
$$+ \frac{\theta_1 R_{pl}^2}{12 P_g \theta_2^3}\left(\theta_1^2 - 4\tau_0\theta_2 + 2P_g\theta_2 R_{pl}\right)^{3/2}$$
$$- \frac{\theta_1}{210 P_g^3 \theta_2^5}\Big[\left(\theta_1^2 - 4\tau_0\theta_2\right.$$
$$+ 2P_g\theta_2 R_C\big)^{5/2}\left(\theta_1^2 - 4\tau_0\theta_2 - 5P_g\theta_2 R_C\right)$$
$$- \left(\theta_1^2 - 4\tau_0\theta_2 + 2P_g\theta_2 R_{pl}\right)^{5/2}\left(\theta_1^2 - 4\tau_0\theta_2 - 5P_g\theta_2 R_{pl}\right)\Big]$$
$$+ \frac{A_2 R_C^2}{2}$$
$$\tag{44}$$

The shear stress at the stenosed arterial wall τ_w can be defined as

$$\tau_w = \left(-\frac{dw_P}{dr}\right)_{r=R_P} + \left(-\frac{dw_B}{dr}\right)_{r=R_B} - \left(-\frac{dw_B}{dr}\right)_{r=R_P} \tag{45}$$

In which on using Eqs. (27) and (28) gives

$$\tau_w = \frac{P_g R_P}{2} + \xi\Big[A_5\left(I_1(\xi R_P) - I_1(\xi R_B)\right)$$
$$- A_6\left(K_1(\xi R_B) - K_1(\xi R_P)\right)\Big] \tag{46}$$

The flow impedance λ is defined as

$$\lambda = \int_0^z \frac{P_g(z)}{Q}\,dz \tag{47}$$

For various values of the parameters involved in this analysis, numerical values of resistance to blood flow can be computed by using the numerical integration on Eq. (47).

4 Special cases

When the blood flows through a constricted artery with porous wall, the velocity profiles for different blood flow models, namely Newtonian–Newtonian, Bingham–Newtonian and Casson–Newtonian are obtained as limiting cases as follows:

4.1 Newtonian–Newtonian fluid model

The velocity distribution of Newtonian–Newtonian fluid model can be calculated by taking the limit of the velocities w_C, w_P, w_B and w_D in Eqs. (26)–(29) as the yield stress (τ_0) and K–L fluid parameter (θ_1) tend to zero. As $\tau_0 \to 0$ and $\theta_1 \to 0$, then the constitutive equation of core (K–L) fluid reduces to the Newtonian viscous fluid, which is given by

$$\tau_{rz} = -\theta_2\left(\frac{\partial w_C}{\partial r}\right) \tag{48}$$

Therefore, the velocity profiles in each layer can be given by

$$w_C = -\frac{P_g r^2}{4\theta_2} + B_2 \tag{49}$$

$$w_P = -\frac{P_g r^2}{4} + B_3 \ln(r) + B_4 \tag{50}$$

$$w_B = B_5 I_0(\xi r) + B_6 K_0(\xi r) + P_g Da \tag{51}$$

$$w_D = P_g Da \tag{52}$$

4.2 Bingham–Newtonian fluid model

The velocity distribution of Bingham–Newtonian fluid model can be calculated by taking the limit of the velocities w_C, w_P, w_B, w_D and w_{pl} in Eqs. (26)–(30) as the K–L fluid parameter (θ_1) tends to zero. As $\theta_1 \to 0$, then the constitutive equation of core (K–L) fluid reduces to the Bingham plastic fluid, which is given by

$$\tau_{rz} = \tau_0 + \theta_2\left(-\frac{\partial w_C}{\partial r}\right) \tag{53}$$

Therefore, the velocity profiles in each layer can be given by

$$w_C = \frac{1}{\theta_2}\left(\tau_0 r - \frac{P_g r^2}{4}\right) + C_2 \tag{54}$$

$$w_P = -\frac{P_g r^2}{4} + C_3 \ln(r) + C_4 \tag{55}$$

$$w_B = C_5 I_0(\xi r) + C_6 K_0(\xi r) + P_g Da \tag{56}$$

$$w_D = P_g Da \tag{57}$$

$$w_{pl} = \frac{1}{\theta_2}\left(\tau_0 R_{pl} - \frac{P_g R_{pl}^2}{4}\right) + C_2 \tag{58}$$

4.3 Casson–Newtonian fluid model

The velocity of distribution Casson–Newtonian fluid model can be calculated by taking the limit of the velocities w_C, w_P, w_B, w_D and w_{pl} in Eqs. (26)–(30) as the K–L fluid parameter (θ_1) tends to $2\sqrt{\tau_0\theta_2}$. If $\theta_1 = 2\sqrt{\tau_0\theta_2}$, then the constitutive equation of core (K–L) fluid reduces to the Casson fluid, which is given by

$$\sqrt{\tau_{rz}} = \sqrt{\tau_0} + \sqrt{\theta_2\left(-\frac{\partial w_C}{\partial r}\right)} \tag{59}$$

Therefore, the velocity profiles in each layer can be given by

$$w_C = -\frac{1}{\theta_2}\left(\tau_0 r + \frac{P_g r^2}{4} - \frac{\sqrt{8\tau_0 P_g}}{3\theta_2}r^{3/2}\right) + D_2 \tag{60}$$

$$w_P = -\frac{P_g r^2}{4} + D_3 \ln(r) + D_4 \tag{61}$$

$$w_B = D_5 I_0(\xi r) + D_6 K_0(\xi r) + P_g Da \tag{62}$$

$$w_D = P_g Da \tag{63}$$

$$w_{pl} = -\frac{1}{\theta_2}\left(\tau_0 R_{pl} + \frac{P_g R_{pl}^2}{4} - \frac{\sqrt{8\tau_0 P_g}}{3\theta_2}R_{pl}^{3/2}\right) + D_2 \tag{64}$$

The expressions for the arbitrary constants B_2–B_6, C_2–C_6 and D_2–D_6 can be obtained as the limiting cases of the arbitrary constants A_2–A_6 for the respective model. It is worth noting that the analytical expressions for velocity profiles [Eqs. (60)–(64)] are coincide with the expressions obtained by Sharma and Yadav [24].

5 Graphical results and discussion

The objective of the present study is to investigate the change in flow pattern due to stenosis and the effect of a porous wall on the blood flow in arterial stenosis whose porous wall is composed of two layers, namely Brinkman and Darcy. It is also intended to bring out the simultaneous effects of non-Newtonian behavior of blood, yield stress, plasma layer thickness, Darcy number, porosity, Darcy slip parameter, and stress jump parameter on physiologically pivotal flow characteristics such as velocity profile, plug core radius, flow flux, wall shear stress, and resistive impedance. For computational purpose, the range of the values of different parameters involved in the present analysis is chosen as [22, 27, 31]: length of the stenosis $L_0 = 1$; location of the stenosis in the axial direction $d = 4$, $z = 4 - 5$; stenosis shape parameter $m = 2 - 5$; maximum height of the stenosis $\delta_s = 0 - 0.2$; porosity $\phi = 0.5$; Darcy slip parameter $\alpha = 0.01 - 0.1$; stress jump parameter $\beta = 0.1$; effective viscosity $\lambda_e = 1.1$; K–L fluid parameters $\theta_1 = 0.2 - 2$, $\theta_2 = 0.8 - 1.2$; yield stress $\tau_0 = 0 - 0.1$; plasma layer thickness $h_P = 0 - 0.1$; Darcy number $Da = 0.01 - 0.1$; Darcy region thickness $h_D = 0.4 - 1.8$.

When the fluid flows in a stenosed artery with porous wall, the velocity profiles for different fluid models such as Newtonian–Newtonian ($\tau_0 = 0, \theta_1 = 0$), Bingham–Newtonian ($\tau_0 = 0.05, \theta_1 = 0$), Casson–Newtonian ($\tau_0 = 0.05, \theta_1 = 0.4899$), and K.L-Newtonian ($\tau_0 = 0.05, \theta_1 = 0.2$ and $\theta_1 = 0.8$) are compared and displayed graphically in Fig. 2. It is obvious that, relative to the fluids with yield stress, the Newtonian fluid velocities are much greater. Another notable observation is that the plot of the velocity profile of Casson fluid ($\tau_0 = 0.05, \theta_1 = \sqrt{2\tau_0\theta_2}$) [24] lies between those of the K.L fluid with $\tau_0 = 0.05, \theta_1 < \sqrt{2\tau_0\theta_2}$ and $\tau_0 = 0.05, \theta_1 > \sqrt{2\tau_0\theta_2}$. Figure 3 shows the radial variation of axial velocity with the yield stress (τ_0) and plasma layer thickness (h_P). It depicts that the axial velocity declines as the yield stress increases. Additionally, it may be observed that with the increase in plasma layer thickness, the axial

Fig. 2 Comparison of the axial velocity profiles in the stenotic zone for various fluid models
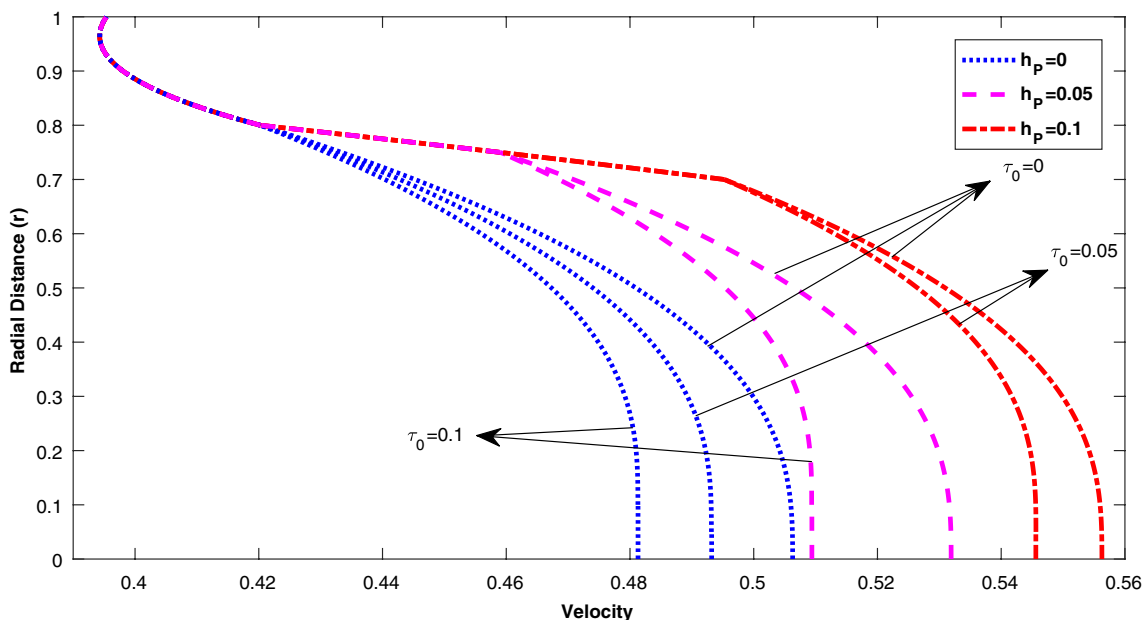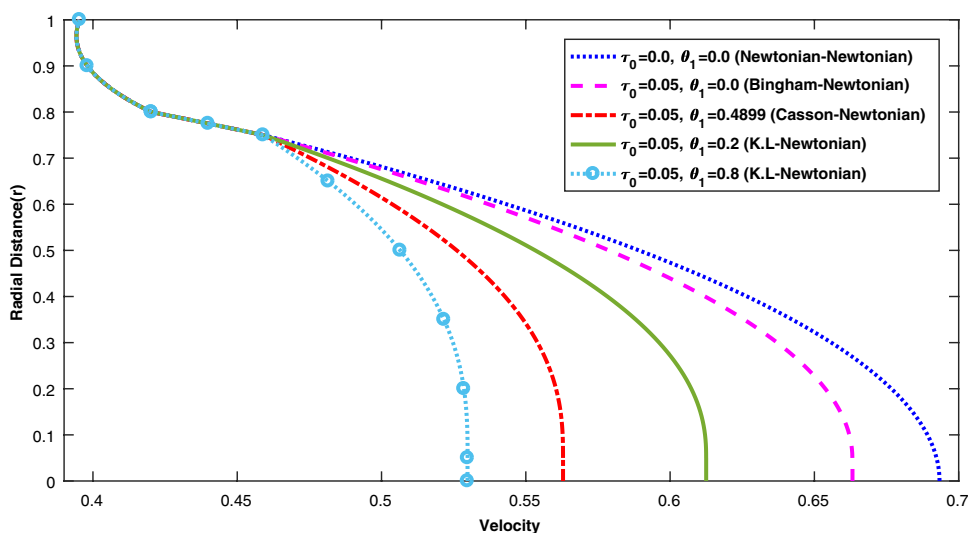

Fig. 3 Radial distribution of blood velocity in the stenotic zone with plasma layer thickness (h_P) and yield stress (τ_0)

velocity continues to increase. The distribution of axial velocity with the radial distance (r) for different values of K–L fluid parameters (θ_1 and θ_2) is shown in Fig. 4. It may be noticed that the rise in the K–L fluid parameters contributes to a decrease in velocity and for the lower values of $\theta_1(\theta_1 < 2)$, the rate of decrease in velocity is observed to be greater.

Figure 5 describes the effect of Darcy number (Da) and Darcy slip parameter (α) on the radial distribution of the axial velocity of the fluid. The figure shows that the velocity of the fluid (blood) in the stenotic region increases rapidly for the higher values of Da, whereas the velocity increases gradually with the increase of α. We infer from the result

that in contrast to the Darcy number, the Darcy slip parameter is a weak parameter in the sense that it induces less variation in the magnitude of the axial velocity. Figure 6 reveals the combined effect of a thickness of Brinkman and Darcy layers on the radial variation of the axial velocity of the fluid. We note that the Brinkman layer thickness (h_B) is altered by the change in the Darcy region thickness (h_D) as the relationship between h_B and h_D is considered to be $h_B = h_D/9$ [27]. It is clear from the figure that the axial velocity in the core, plasma, and Brinkman regions increases as the thickness of the Darcy region decreases, but it starts to decrease at the end of the Brinkman region.

Fig. 4 Variation of velocity of blood with parameter constants in K–L fluid (θ_1 and θ_2) in the stenotic zone
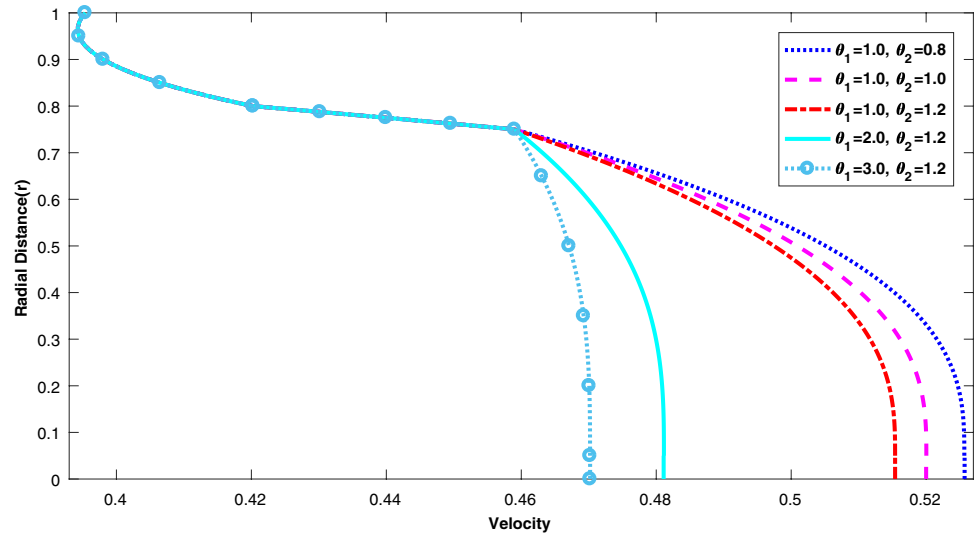
Fig. 5 Distribution of blood velocity in the stenotic zone with Darcy number (Da) and slip parameter of Darcy (α)
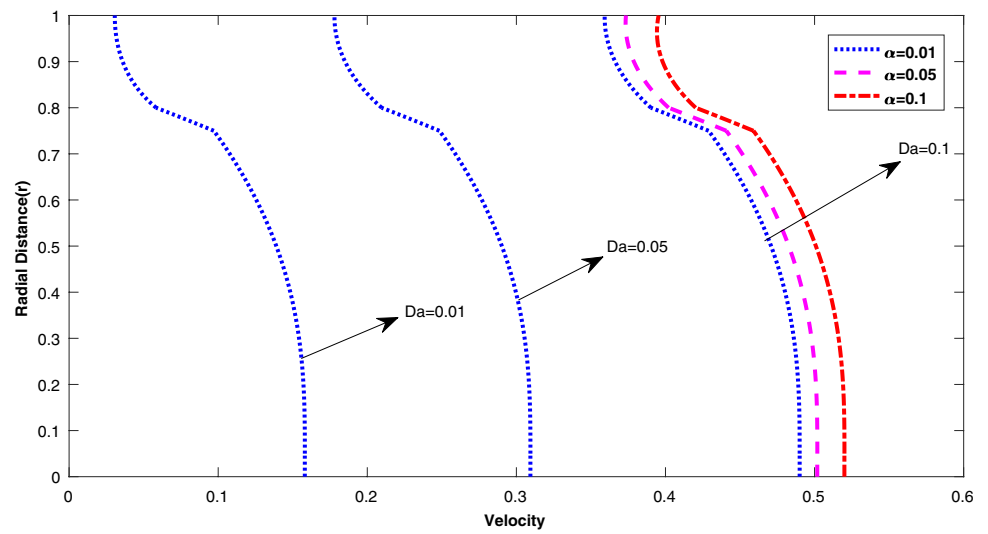
Fig. 6 Distribution of velocity of blood in the stenotic zone with Darcy layer thickness (h_D)
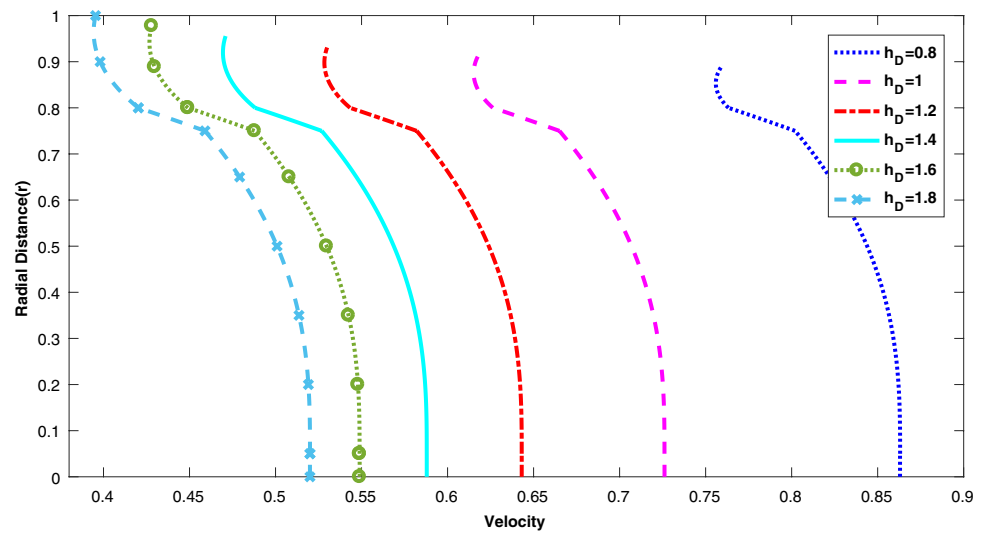
It is noticed that the axial velocity is very much decreased as yield stress increases, and therefore the plug flow becomes prominent in the flow of blood. The effects of various parameters (τ_0, h_P, θ_1, Da, α, h_D, δ_s, and m) on the plug flow radius (R_{pl}) are shown in Figs. 7, 8, 9, 10, 11 and 12. It is illustrative that as z increases from 4 to 4.5, the plug flow radius decreases, and as z increases from 4.5 to 5, it increases. It can be observed from Figs. 7 and 8 that the plug core radius (R_{pl}) increases when yield stress increases

and the same behavior is noted as plasma layer thickness (h_P) increases, whereas its variation with δ_s is always having an opposite nature when other parameters are held fixed. Further, one notices from Fig. 8 that the plug core radius is found to be constant along the axial direction (z) in the absence of stenosis ($\delta_s = 0$).

The effect of parameter constant in K–L model fluid (θ_1) on plug core radius along the axial direction is shown in Fig. 9. It may be pointed out that the plug core radius
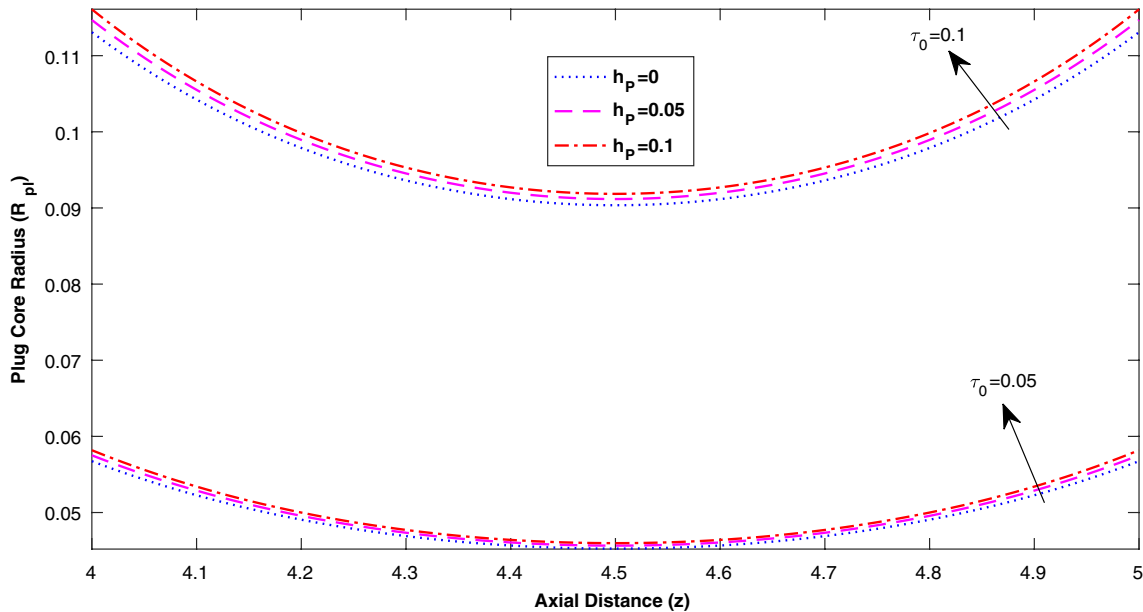
Fig. 7 Axial distribution of plug flow radius (R_{pl}) with plasma layer thickness (h_P) and yield stress (τ_0)
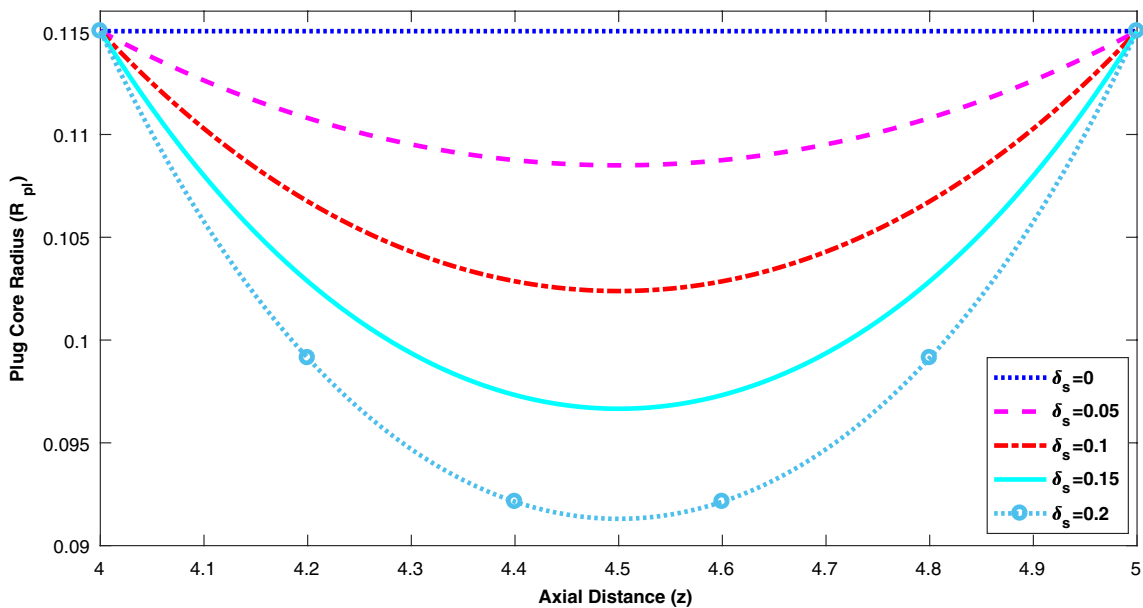
Fig. 8 Axial variation of plug flow radius (R_{pl}) with the maximal constriction height (δ_s)
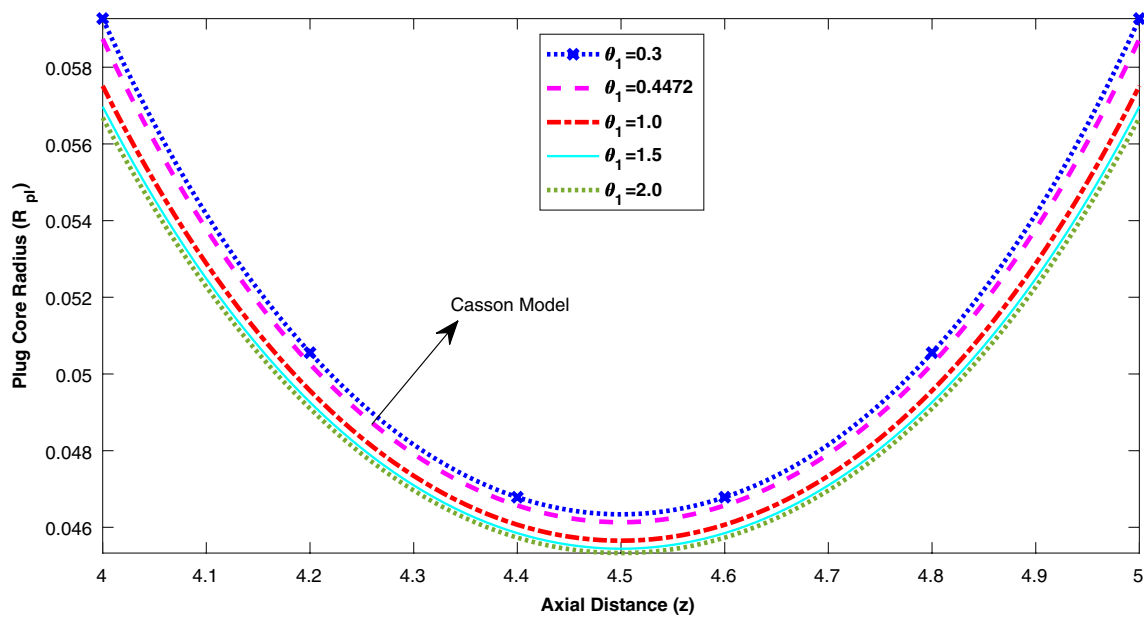
Fig. 9 Axial distribution of plug flow radius (R_{pl}) with the K–L fluid parameter (θ_1)
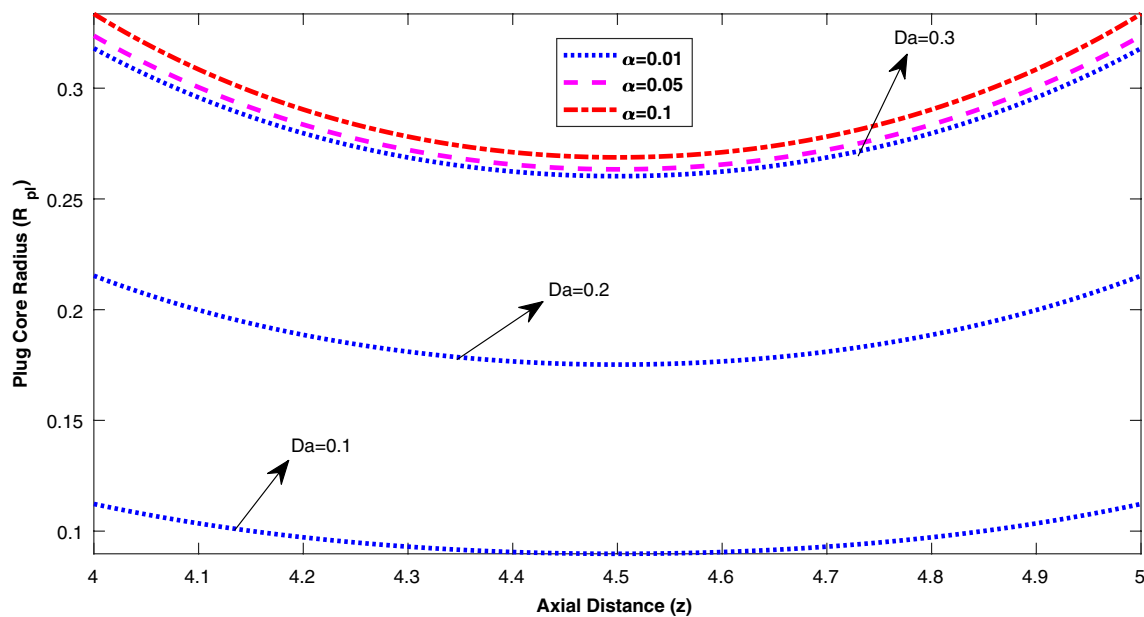
Fig. 10 Axial distribution of plug flow radius (R_{pl}) with Darcy number (Da) and slip parameter of Darcy (α)

increases as θ_1 decreases. Figure 10 sketches the variation of plug core radius along the axial direction with Darcy number (Da) and Darcy slip parameter (α). It is clear from the results that the plug core radius enhances with the increase in the values of Da and α. Figure 11 shows that the joint impact of the thickness of the Darcy region (h_D) and Brinkman layer (h_B) on the plug core radius. It may be noted that as the value of h_D raises, the plug core radius upgrades. Figure 12 reveals that the plug core radius

escalates in the upstream region of the constriction and reaches its minimum value at some stage, and further, it decreases in the downstream region with the advancement in the value of stenotic shape parameter (m). Also, it is seen that the point at which the plug core radius takes the least value is shifting towards downstream along the axial direction as the value of n increases, which forms the new evidence added to the literature.
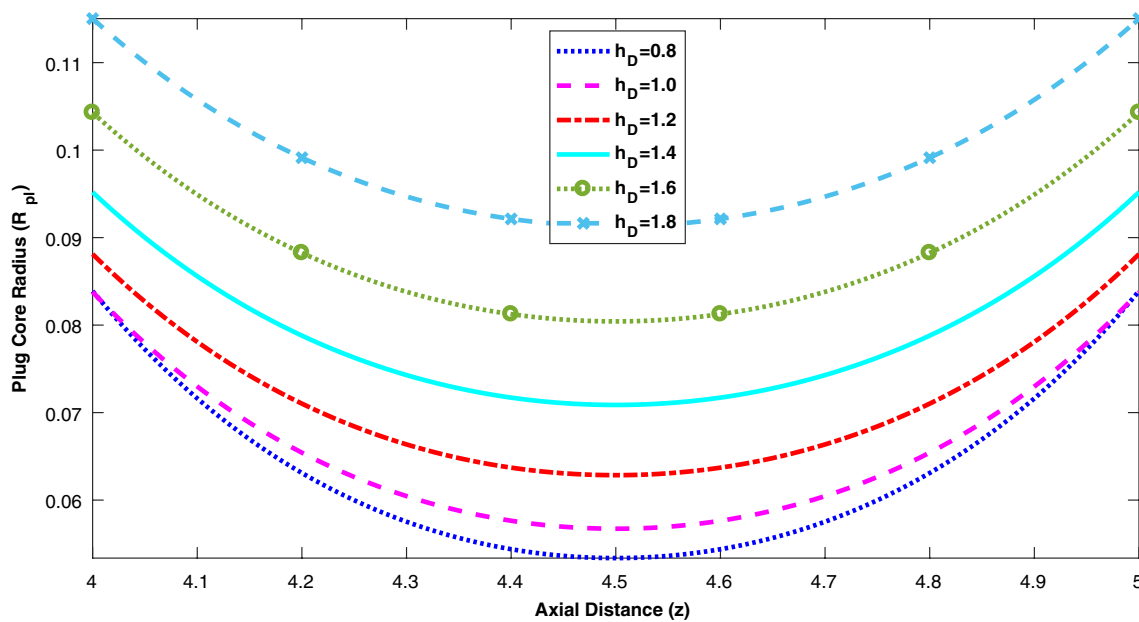
Fig. 11 Axial variation of plug flow radius (R_{pl}) with the thickness of Darcy region (h_D)
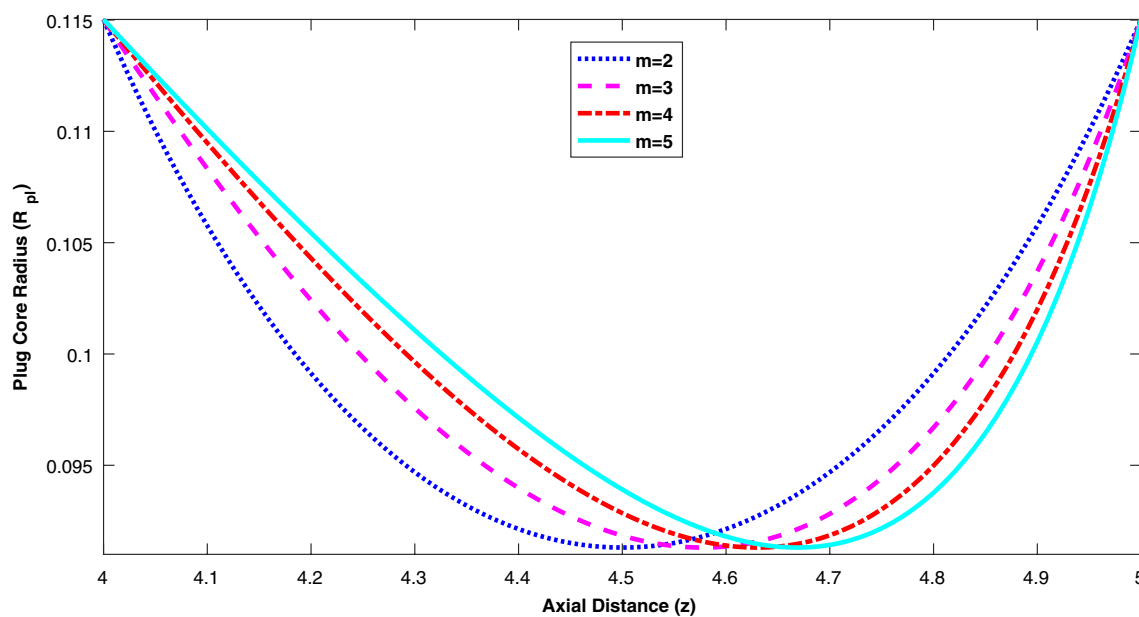
Fig. 12 Axial variation of plug flow radius (R_{pl}) for different values of shape parameter of constriction (m)

Wall shear stress or skin friction signifies a tangential force applied to the wall of the blood vessel by the flowing blood which is produced because of the traction between the wall and the fluid (blood) along the wall. The axial variation of wall shear stress (τ_w) for different values of τ_0, h_P, θ_1, Da, α and m in the stenotic region has been studied and illustrated in Figs. 13, 14, 15, 16, and 17. Figure 13 shows the variation of the wall shear stress with z-axis for different values of the yield stress (τ_0) and thickness of the plasma layer (h_P). It is observed that the shear stress at the arterial wall decreases as the plasma layer thickness increases while it increases with the enhancement in yield stress for a fixed value of h_P. It is noticed that the rate of increase or decrease of wall shear stress with respect to the tube axis is found to be higher in the case of yield stress in comparison with the plasma layer thickness. Figure 14 is drawn to analyze the influence of parameter constant in K–L fluid (θ_1) on the axial variation of skin friction. It is
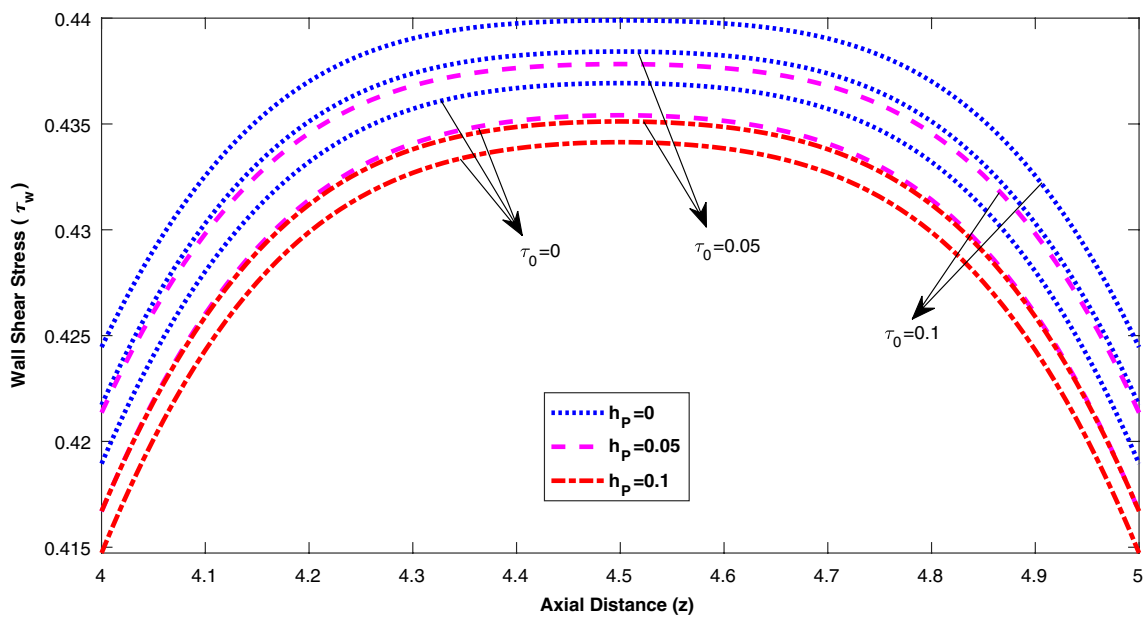
Fig. 13 Axial distribution of wall shear stress (τ_w) with plasma layer thickness (h_P) and yield stress (τ_0)
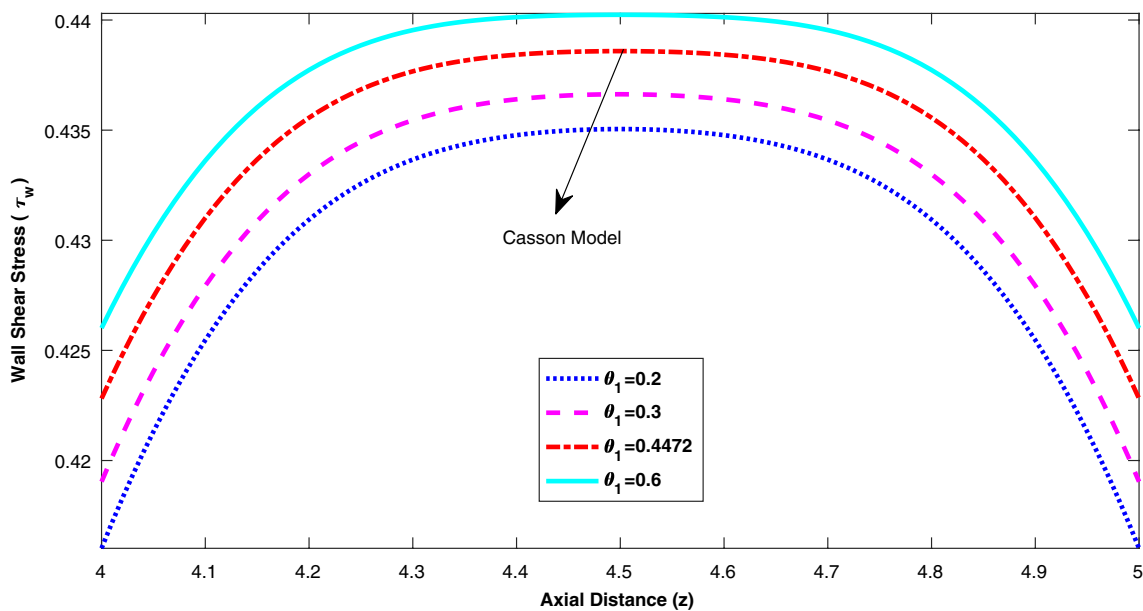

Fig. 14 Axial variation of wall shear stress (τ_w) with parameter constant in K–L fluid (θ_1)

established that the skin friction in axial direction increases considerably with the increase of parameter constant in K–L fluid (θ_1). One can see that as *z* moves from 4 to 4.5, the skin friction along the axial direction upsurges, and then it declines symmetrically as *z* moves further from 4.5 to 5.

In Fig. 15, how the combined role of Darcy number (*Da*) and Darcy slip parameter (α) in changing the pattern of skin friction (τ_w) has been displayed. It is seen that the

skin friction decreases rapidly with the increase of Darcy number (*Da*), but it decays marginally as the Darcy slip parameter (α) increases for a fixed value of *Da*. Figure 16 is drawn to explore the combined effect of the thickness of Brinkman layer (h_B) and Darcy region (h_D) on the skin friction. When the value of $h_D \leq 1.0$, the wall shear stress increases, and it starts decreasing for $h_D > 1.0$. Therefore, the understanding of the joint role of h_B and h_D may be helpful in normalizing the blood flow. The drive of Fig. 17
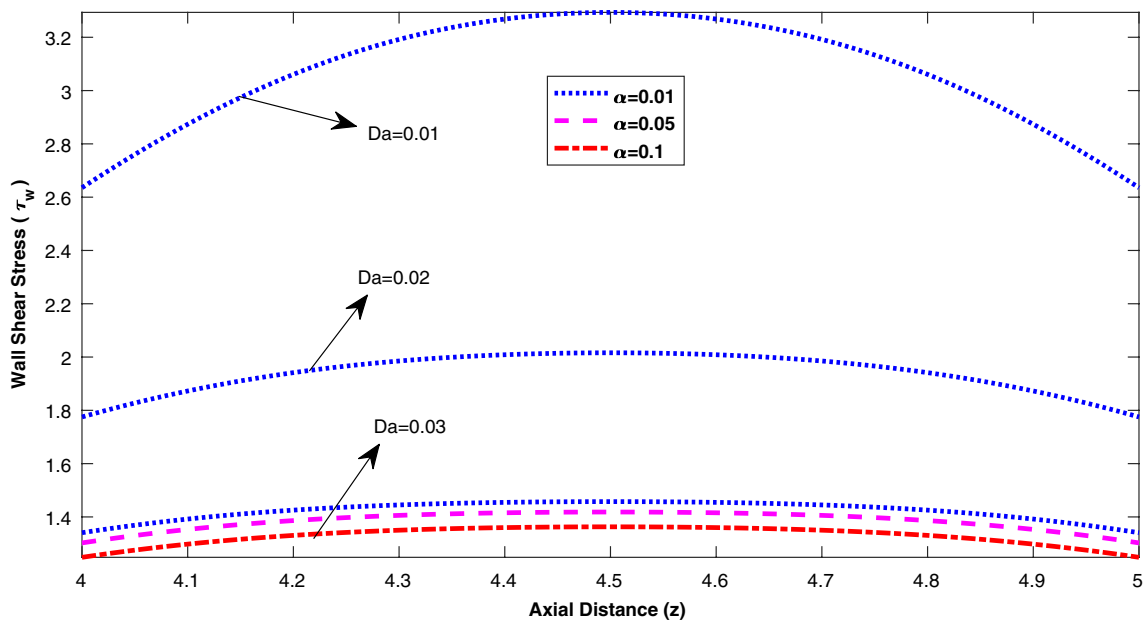
Fig. 15 Axial variation of wall shear stress (τ_w) in the stenotic zone for different values of Darcy number (Da) and slip parameter of Darcy (α)
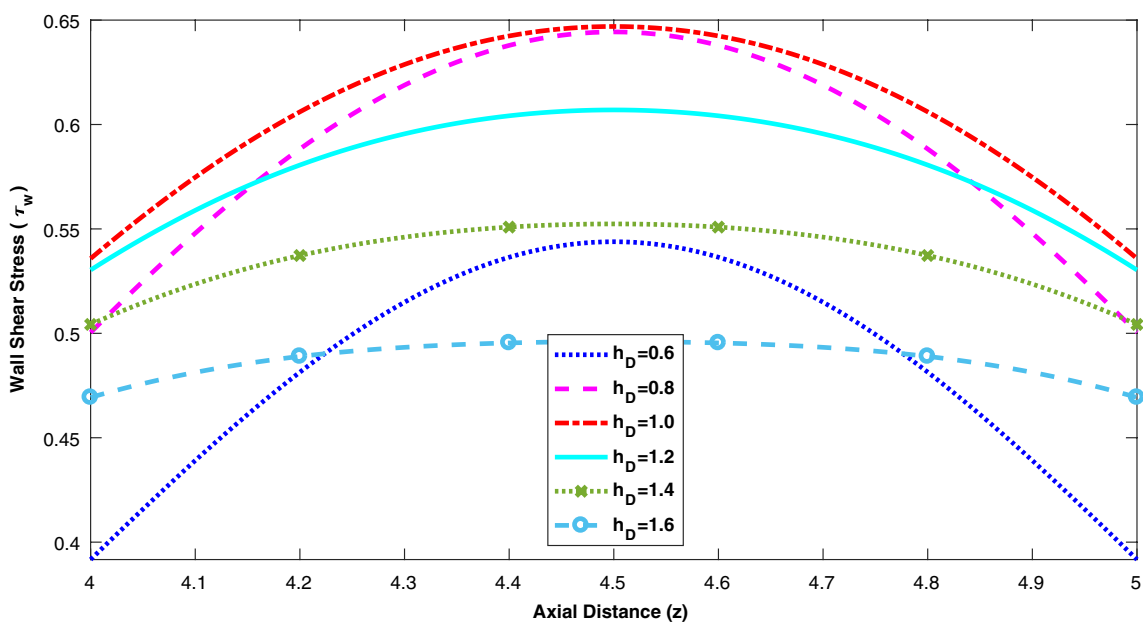

Fig. 16 Wall shear stress (τ_w) distribution in the stenotic zone for different values of the Darcy region thickness (h_D)

is to illustrate the effect of stenosis shape parameter (m) on the axial distribution of skin friction. It is important to note that in the upstream of the stenotic zone, skin friction decreases and then increases in the downstream of the region as the m value increases. A rise in the magnitude of m tends to change the position where the wall shear stress achieves its maximum towards the downstream.

For more insight into the physical characteristics of the shear stress on the wall geometry of the artery, the response of shear stress in separate regions and total wall shear stress for the two cases such as $\delta_s = 0.0$ (uniform artery) and $\delta_s = 0.1$ (stenosed artery) is depicted in Table 1. From this table, we can see that the magnitude of shear stress is positive at the end of the plasma layer $\left(\left(\tau_w\right)_P > 0\right)$, whereas it is negative in the Brinkman region $\left(\left(\tau_w\right)_B < 0\right)$. It is due to the fact that the axial velocity profiles continue to decrease till the end of the plasma layer, and increase gently in the Brinkman region (see Figs. 2, 3, 4, 5 and 6).
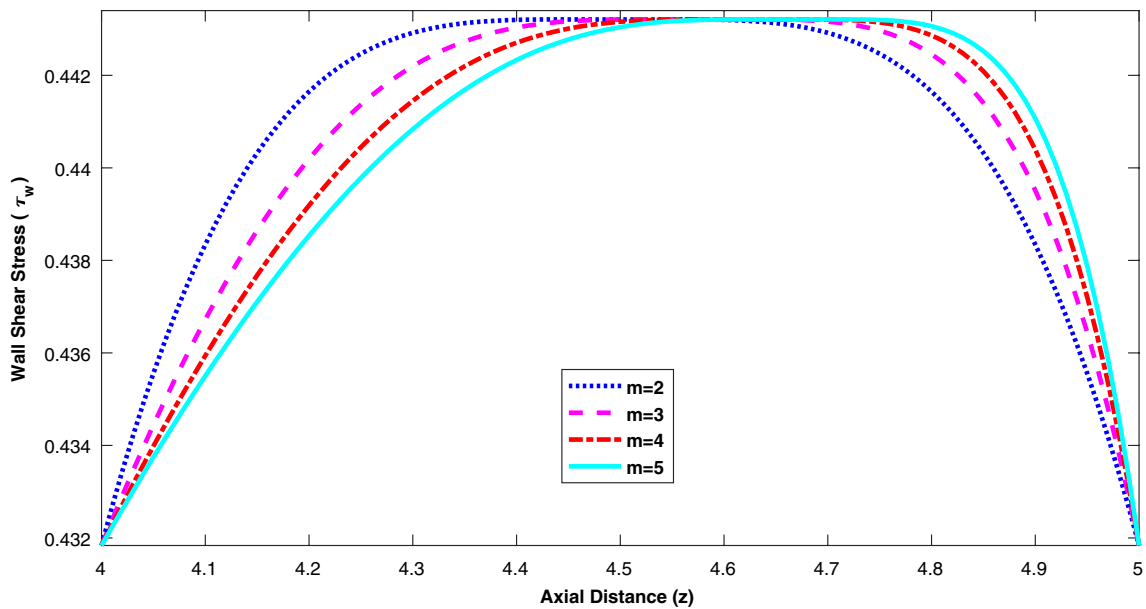
Fig. 17 Axial variation of wall shear stress (τ_w) in the stenotic region for different values of shape parameter of constriction (m)

However, the magnitude of total shear stress (τ_w) exerted by the flowing blood on the porous wall of the artery is positive, and is observed to be higher in the case of stenosed arteries as compared to the uniform vessels.

The axial variation of resistive impedance (λ) experienced by the flow of blood is shown in Figs. 18, 19, 20, 21 and 22 for various values of the critical parameters involved in the study. The joint effect of yield stress (τ_0) and plasma layer thickness (h_P) on flow impedance has been studied from Fig. 18. The resistance to flow enhances as the yield stress (τ_0) increases for a fixed value of h_P, whereas its variation with plasma layer thickness (h_P) is of inverse nature. Figure 19 displays the axial distribution of the resistive force (flow impedance) for different values of parameter constant in K–L fluid (θ_1). It is seen that the flow resistance is increased as the value of parameter constant in K–L fluid increases. Figure 20 exhibits the combined effect of the thickness of the Brinkman layer
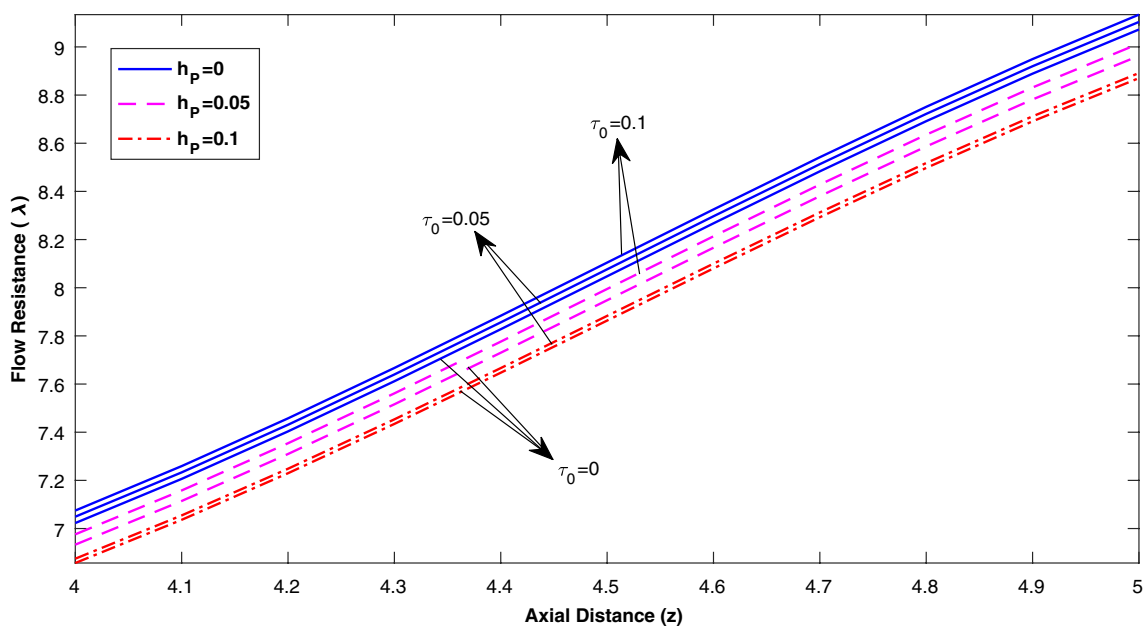

Fig. 18 Axial variation of flow resistance (λ) with plasma layer thickness (h_P) for different values of yield stress (τ_0) in the stenotic zone
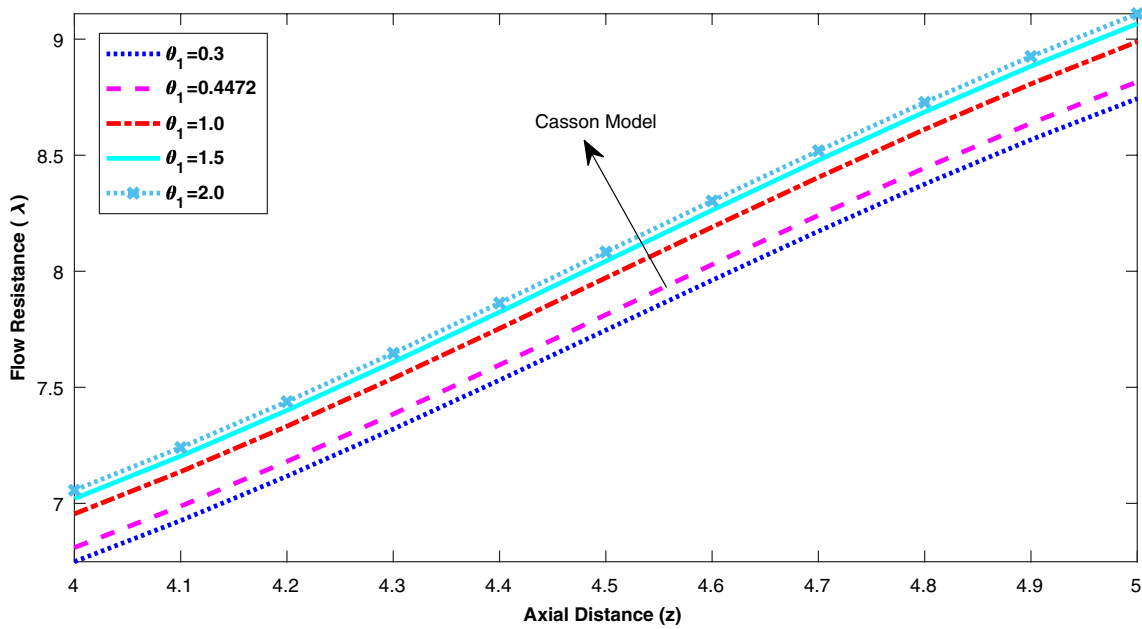
Fig. 19 Distribution of flow impedance (λ) in the stenotic zone for different values of parameter constant in K–L fluid (θ_1)

Table 1 Shear stress on the wall geometry in separate regions for different values of stenotic height

δ_s	$(\tau_w)_P = \left(-\dfrac{dw_P}{dr}\right)_{r=R_P}$	$(\tau_w)_B = \left(-\dfrac{dw_B}{dr}\right)_{r=R_B} - \left(-\dfrac{dw_B}{dr}\right)_{r=R_P}$	$\tau_w = (\tau_w)_P + (\tau_w)_B + (\tau_w)_D$
0.0	0.869370	-0.437533	0.431837
0.1	0.879048	-0.438842	0.440206
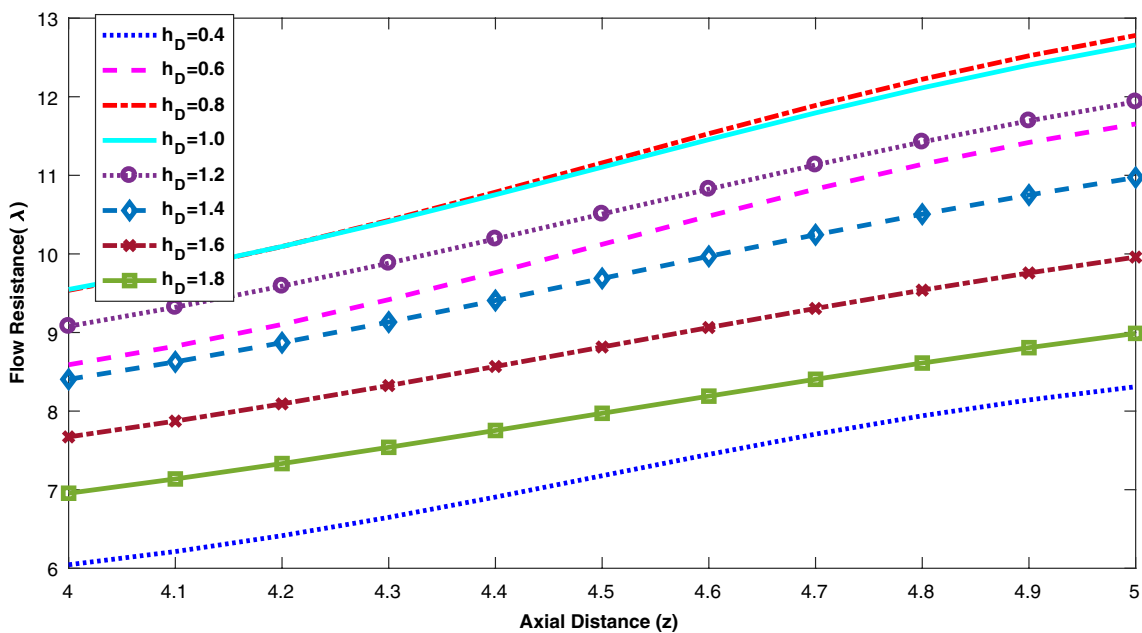
Fig. 20 Axial variation of resistive impedance (λ) in the stenotic zone with the Darcy region thickness (h_D)
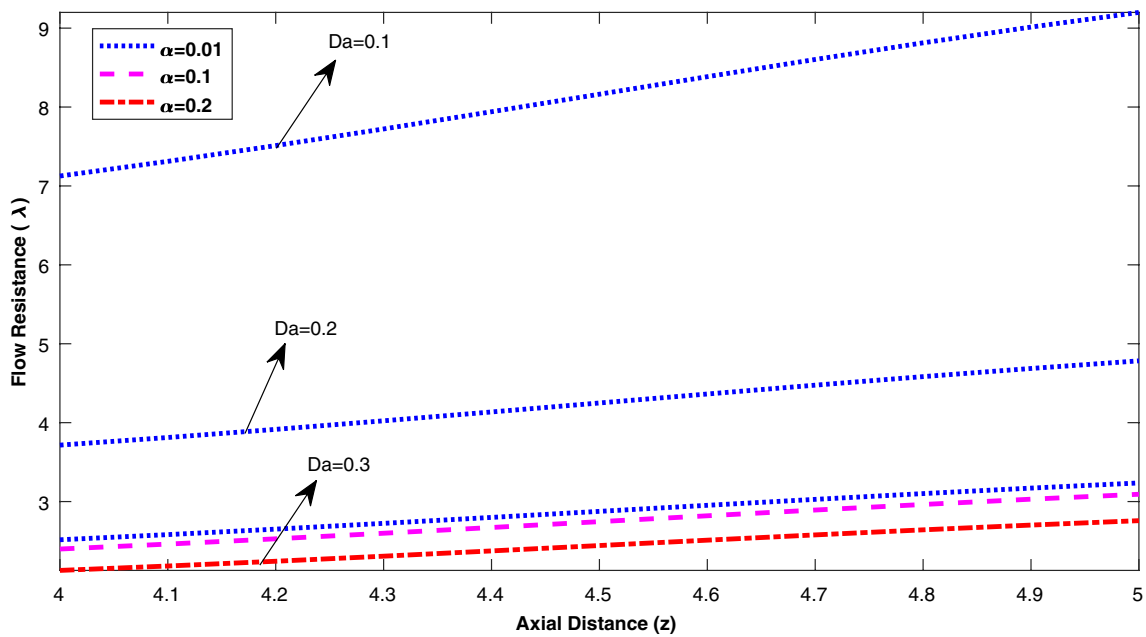
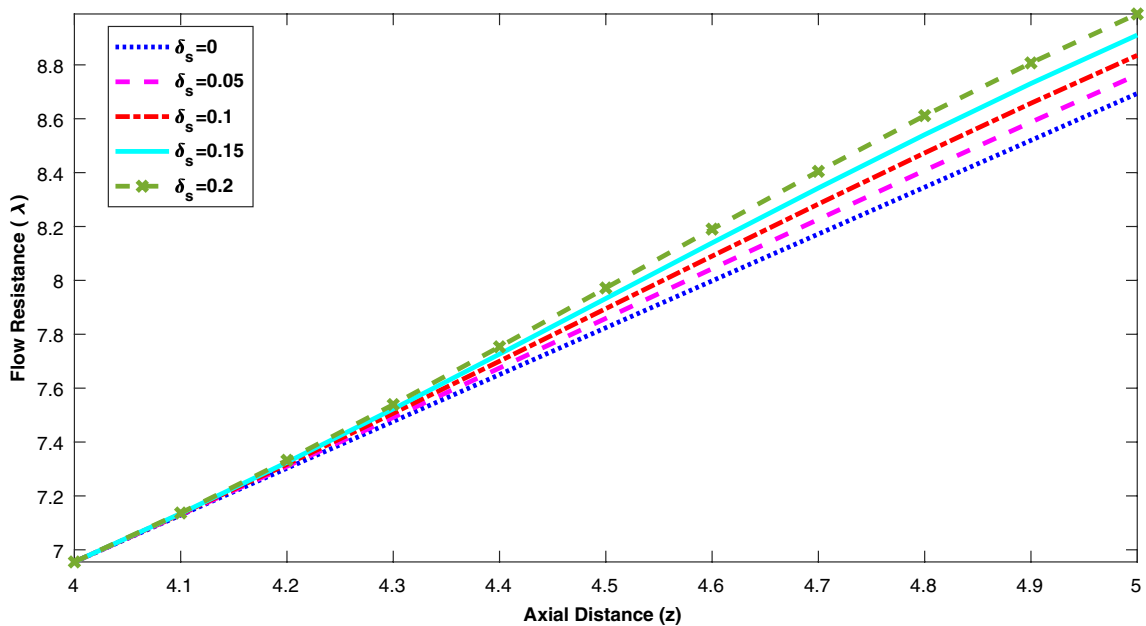**Fig. 21** Variation of flow impedance (λ) in the stenotic zone with the Darcy number (Da) and slip parameter of Darcy (α)

Fig. 22 Axial variation of resistive impedance (λ) with the maximal stenotic height (δ_s)

(h_B) and Darcy region (h_D) on the resistive impedance. As the value of $h_D \leq 0.8$, the flow resistance increases while it has an opposite nature when $h_D > 0.8$. Thus, the collective relevant role of h_B and h_D could be provided suitable eminence in updating the blood flow model.

Figure 21 is drawn to see the influence of Darcy number (Da) and parameter of Darcy slip (α) on the axial distribution of resistive impedance. One can easy to observe that the impedance to flow decays rapidly as the Darcy number (Da) enhances, but it decreases marginally with the rise of the parameter of Darcy slip (α) for a fixed value of Da. Figure 22 depicts how the flow resistance is affected by the severity of the constriction. The maximal constriction height has been modified by the variation of

parameter δ_s. It is found that for $\delta_s = 0$, i.e., when there is blood flow through the artery in the absence of stenosis (uniform artery), the curve representing the variation of the flow impedance becomes perfectly linear. This linearity of the results is gradually lost with enhancing the maximal constriction height (δ_s), and the results are observed to grow nonlinear. Further, one can see that the flow impedance increases gradually throughout the constricted region as the maximum height of the constriction (δ_s) increases. These interpretations are self-explanatory in the sense that when the maximal stenotic height (δ_s) is drastically changed, say for $\delta_s = 0.2$, the resistive force exerted by the streaming blood appears, as predicted, to be a maximum. Hence, the height of the constriction plays

a vital role in the flow impedance encountered to characterize the flow behavior of blood in a stenosed artery.

To get more insight into the flow behavior, streamlines are plotted for the whole region in Figs. 23 and 24. The impact of the thickness of the porous wall on the streamline pattern is shown in Fig. 23. As the Darcy region thickness increases from $h_D = 0.6$ to $h_D = 1.2$, the number of bolus increases but the size of the trapping bolus diminishes, whereas the inverse behavior of the streamline pattern is noticed in the Brinkman region. Figure 24 elucidates that the blood flow pattern (streamlines) in the stenotic region when the stenosis shape changes from symmetric ($m = 2$) to asymmetric ($m = 5$). It is observed from this pattern that the trapping bolus is shifting towards the downstream along the z-axis as the value of m increases.
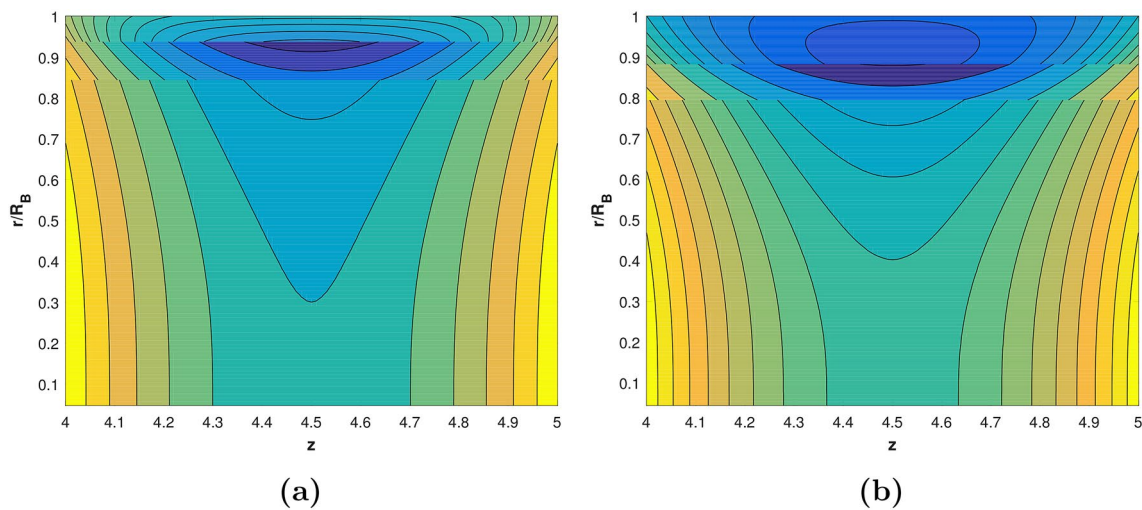

(a)   (b)

Fig. 23 Streamlines for different values of Darcy region thickness: **a** $h_D = 0.6$, **b** $h_D = 1.2$

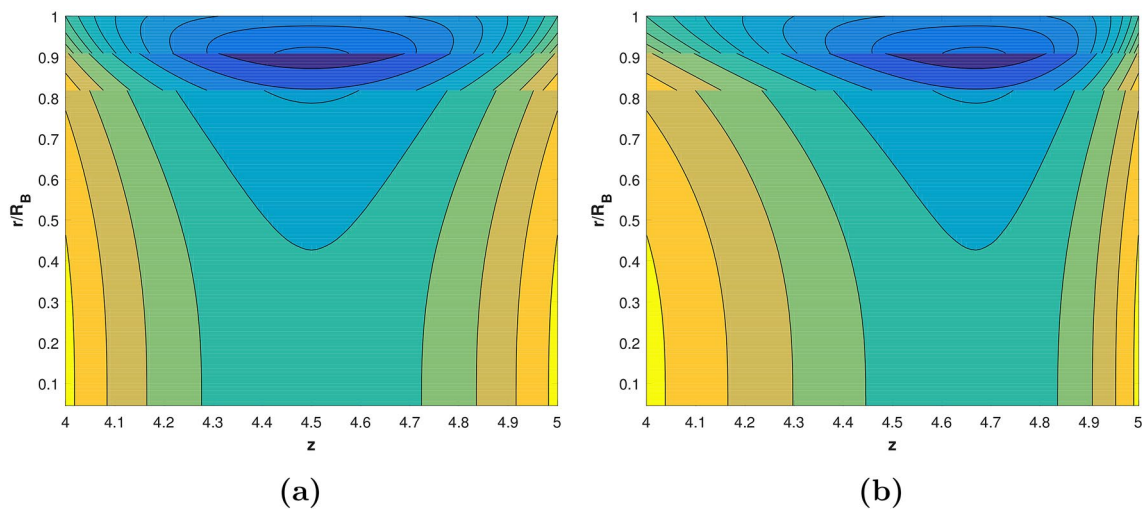(a)   (b)

Fig. 24 Streamlines for different values of stenosis shape parameter: **a** $m = 2$, **b** $m = 5$

6 Conclusion

The theoretical study of a two-fluid model of blood flow in a stenosed artery with porous wall treating blood in the core region as non-Newtonian fluid and peripheral plasma, Brinkman and Darcy regions filled with Newtonian fluid has been done in the present work. Due to the presence of the Brinkman and Darcy layers in the porous wall, the study brings out several curious fluid mechanical phenomena. It is found that blood velocity in the stenotic region attenuates with the increasing values of the K–L fluid parameters. Further, the velocity in both plug flow and non-plug flow regions increases with the increase of plasma layer thickness, but it slows down by the yield stress.

The plug core radius rises in the upstream region of the constriction, and then it dwindles in the downstream region with the enhancement in the value of the shape parameter of constriction (m). Further, the point at which the plug core radius takes a minimum value is shifting towards downstream along the axial direction as the value of m enhances. The flow impedance and skin friction exerted by the streaming blood are found to reduce with the increasing values of Darcy number and Darcy slip parameter, but they are enhanced with the K–L fluid parameter. The precious outcome of the present study is that the joint effect of thickness of the Brinkman layer and the Darcy region on the skin friction and flow impedance. It is found that for lower values of h_D (Darcy region thickness), the skin friction and resistive impedance are enhanced with the rise in h_D, while these are found to be opposite nature for higher values of h_D, which forms the new information, at least to the authors' knowledge, added to the literature. Hence, looking at the significance of the hemodynamic factors in the understanding of blood flow in stenosed arteries, we can conclude that the information about the effects of the rheology of K–L fluid, the thickness of the plasma layer and porous wall on the flow characteristics and the precious way of selecting the appropriate dimensional values of these parameters mentioned above can be utilized to normalize the blood flow in the abnormal arteries and lead to the development of new diagnostic tools.

Declarations

Conflict of interest The authors declare that they have no conflict of interest.

Appendix

The system of algebraic Eqs. (32)–(35) have been solved by using general Matlab code and therefore, the explanations for the arbitrary constants (A_2, A_4, A_5 and A_6) can be obtained as

$$
\begin{aligned}
A_2 = \Big(& 2\alpha\beta\phi\theta_1^3\Delta(I_0(\xi R_P)K_0(\xi R_B) \\
& - I_0(\xi R_B)K_0(\xi R_P)) + 2\xi^2 Da\theta_1^3\Delta(I_1(\xi R_B)K_1(\xi R_P) \\
& - I_1(\xi R_P) \\
& K_1(\xi R_B)) - 2\alpha\xi\sqrt{Da}\theta_1^3\Delta(I_1(\xi R_P)K_0(\xi R_B) \\
& + I_0(\xi R_B)K_1(\xi R_P)) + 2\beta\xi\phi\sqrt{Da}\theta_1^3\Delta(I_1(\xi R_B) \\
& K_0(\xi R_P) + I_0(\xi R_P)K_1(\xi R_B)) \\
& + 6\alpha\beta\phi P_g R_C\theta_2\theta_1^2(I_0(\xi R_B)K_0(\xi R_P) \\
& - I_0(\xi R_P)K_0(\xi R_B)) + 6\xi^2 \\
& DaP_g R_C\theta_2\theta_1^2(I_1(\xi R_P)K_1(\xi R_B) \\
& - I_1(\xi R_B)K_1(\xi R_P))
\end{aligned}
$$

$$
\begin{aligned}
& + 6\alpha\xi P_g R_C\theta_2\theta_1^2\sqrt{Da}(I_1(\xi R_P)K_0(\xi R_B) \\
& + I_0(\xi R_B)K_1(\xi R_P)) \\
& - 6\beta\xi\phi\sqrt{Da}P_g R_C\theta_2\theta_1^2(I_1(\xi R_B)K_0(\xi R_P) \\
& + I_0(\xi R_P)K_1(\xi R_B)) + 4\alpha\beta\phi P_g \\
& R_C\theta_1\theta_2\Delta(I_0(\xi R_P)K_0(\xi R_B) - I_0(\xi R_B)K_0(\xi R_P)) \\
& + 4\xi^2 DaP_g R_C\theta_1\theta_2\Delta(I_1(\xi R_B)K_1(\xi R_P) \\
& - I_1(\xi R_P)K_1(\xi R_B)) \\
& - 4\alpha\xi\sqrt{Da}P_g R_C\theta_1\theta_2\Delta(I_1(\xi R_P)K_0(\xi R_B) \\
& + I_0(\xi R_B)K_1(\xi R_P)) + 4\beta\xi\phi P_g \\
& \sqrt{Da}R_C\theta_1\theta_2\Delta(I_1(\xi R_B)K_0(\xi R_P)
\end{aligned}
$$

$+ I_0(\xi R_P)K_1(\xi R_B))$

$+ 8\alpha\beta\phi\theta_1\theta_2\tau_0\Delta(I_0(\xi R_B)K_0(\xi R_P)$

$- I_0(\xi R_P)K_0(\xi R_B))$

$+ 8\xi^2 Da\theta_1\theta_2\tau_0\Delta(I_1(\xi R_P)K_1(\xi R_B)$

$- I_1(\xi R_B)K_1(\xi R_P))$

$+ 8\alpha\xi\sqrt{Da}\theta_1\theta_2$

$\tau_0\Delta(I_1(\xi R_P)K_0(\xi R_B) + I_0(\xi R_B)K_1(\xi R_P))$

$- 8\beta\xi\phi\sqrt{Da}\theta_1\theta_2\tau_0\Delta(I_1(\xi R_B)K_0(\xi R_P) + I_0(\xi R_P)$

$K_1(\xi R_B)) + 12\xi^2 Da^2 P_g^2\theta_2^3(I_1(\xi R_B)K_1(\xi R_P)$

$- I_1(\xi R_B)K_1(\xi R_P)) + 12\alpha\xi Da^{3/2}P_g^2\theta_2^3(I_1(\xi R_P)$

$K_0(\xi R_B) + I_0(\xi R_B)K_1(\xi R_P))$

$+ 3\alpha\beta\phi(I_0(\xi R_P)K_0(\xi R_B)$

$- I_0(\xi R_P)K_0(\xi R_P))P_g^2\theta_2^3 R_C^2 + 3\xi^2$

$DaP_g^2 R_C^2\theta_2^3(I_1(\xi R_B)K_1(\xi R_P)$

$- I_1(\xi R_P)K_1(\xi R_B))$

$- 3\alpha\xi\sqrt{Da}P_g^2(I_1(\xi R_P)K_0(\xi R_B) - I_0(\xi R_B)$

$K_1(\xi R_P))R_C^2\theta_2^3$

$+ 3\beta\xi\phi\sqrt{Da}P_g^2 R_C^2\theta_2^3(I_1(\xi R_B)K_0(\xi R_P)$

$+ I_0(\xi R_P)K_1(\xi R_B))$

$+ 3\alpha\beta\phi P_g^2 R_P^2\theta_2^3$

$(I_0(\xi R_B)K_0(\xi R_P) - I_0(\xi R_P)K_0(\xi R_B))$

$+ 3\xi^2 DaP_g^2\theta_2^3(I_1(\xi R_P)K_1(\xi R_B)$

$- I_1(\xi R_P)K_1(\xi R_P))$

$R_P^2 + 3\alpha\xi\sqrt{Da}P_g^2 R_P^2\theta_2^3(I_1(\xi R_P)K_0(\xi R_B)$

$+ I_0(\xi R_B)K_1(\xi R_P)) - 3\beta\xi\phi\sqrt{Da}P_g^2 R_P^2\theta_2^3(I_1(\xi R_B)$

$K_0(\xi R_P) - I_0(\xi R_P)K_1(\xi R_B))$

$- 6\xi\phi DaP_g^2 R_P\theta_2^3(I_1(\xi R_B)K_0(\xi R_P)$

$+ I_0(\xi R_P)K_1(\xi R_B)) + 6\alpha$

$\phi\sqrt{Da}P_g^2 R_P\theta_2^3(I_0(\xi R_B)K_0(\xi R_P)$

$- I_0(\xi R_P)K_0(\xi R_B))$

$+ 3\alpha\beta\phi P_g^2 R_C^2\theta_2^2(I_0(\xi R_B)K_0(\xi R_P)$

$- I_0(\xi R_P)K_0(\xi R_B))$

$+ 3\xi^2 DaP_g^2 R_C^2\theta_2^2(I_1(\xi R_P)K_1(\xi R_B)$

$- I_1(\xi R_B)K_1(\xi R_P)) + 3\alpha\xi\sqrt{Da}P_g^2$

$R_C^2\theta_2^2(I_1(\xi R_P)K_0(\xi R_B) + I_0(\xi R_B)K_1(\xi R_P))$

$- 3\beta\xi(I_1(\xi R_B)K_0(\xi R_P)$

$+ I_0(\xi R_P)K_1(\xi R_B))$

$\phi\sqrt{Da}P_g^2 R_C^2\theta_2^2$

$+ 12\alpha\beta\phi P_g R_C\theta_2^2\tau_0(I_0(\xi R_P)K_0(\xi R_B)$

$- I_0(\xi R_B)K_0(\xi R_P)) + 12\xi^2 DaP_g R_C\theta_2^2\tau_0$

$(I_1(\xi R_B)K_1(\xi R_P) - I_1(\xi R_P)K_1(\xi R_B))$

$- 12\alpha(I_1(\xi R_B)K_0(\xi R_B)\sqrt{Da}$

$+ I_0(\xi R_B)K_1(\xi R_P))$

$\xi\sqrt{Da}P_g R_C\theta_2^2\tau_0$

$+ 12\beta\xi\phi\sqrt{Da}P_g R_C\theta_2^2\tau_0(I_1(\xi R_B)K_0(\xi R_P)$

$+ I_0(\xi R_P)K_1(\xi R_B)))/12\theta_2^3 P_g$

$\Big(\alpha\xi\sqrt{Da}(K_0(\xi R_B)I_1(\xi R_P) + I_0(\xi R_B)K_1(\xi R_P))$

$- \beta\xi\phi\sqrt{Da}(I_1(\xi R_B)K_0(\xi R_P) + K_1(\xi R_B)$

$I_0(\xi R_P)) + \xi^2 Da(K_1(\xi R_B)I_1(\xi R_P)$

$- I_1(\xi R_B)K_1(\xi R_P)) + \alpha\beta\phi(I_0(\xi R_B)K_0(\xi R_P)$

$- K_0(\xi R_B)I_0(\xi R_P))\Big)$

$A_4 = \Big(2\alpha P_g\phi\sqrt{Da}R_P(I_0(\xi R_B)K_0(\xi R_P) - K_0(\xi R_B)I_0(\xi R_P))$

$\quad + 4\alpha\xi P_g Da^{3/2}(K_0(\xi R_B)I_1(\xi R_P)$

$\quad + I_0(\xi R_B)K_1(\xi R_P)) + \alpha\xi P_g\sqrt{Da}R_P^2(K_0(\xi R_B)I_1(\xi R_P)$

$\quad + I_0(\xi R_B)K_1(\xi R_P))$

$\quad - \beta\xi P_g\phi\sqrt{Da}R_P^2(I_1(\xi R_B)K_0(\xi R_P)$

$\quad + K_1(\xi R_B)I_0(\xi R_P)) + 4\xi^2 P_g Da^2(K_1(\xi R_B)I_1(\xi R_P)$

$\quad - I_1(\xi R_B)K_1(\xi R_P)) + \xi^2 P_g DaR_P^2(K_1(\xi R_B)I_1(\xi R_P)$

$\quad - I_1(\xi R_B)K_1(\xi R_P))$

$\quad - 2\xi P_g\phi DaR_P(I_1(\xi R_B)K_0(\xi R_P)$

$\quad + K_1(\xi R_B)I_0(\xi R_P)) + \alpha\beta P_g\phi R_P^2(I_0(\xi R_B)K_0(\xi R_P)$

$\quad - K_0(\xi R_B)I_0(\xi R_P))\Big)/4\Big(\alpha\xi\sqrt{Da}(K_0(\xi R_B)I_1(\xi R_P)$

$\quad + I_0(\xi R_B)K_1(\xi R_P))$

$\quad - \beta\xi\phi\sqrt{Da}(I_1(\xi R_B)K_0(\xi R_P) + K_1(\xi R_B)I_0(\xi R_P))$

$\quad + \xi^2 Da(K_1(\xi R_B)I_1(\xi R_P)$

$\quad - I_1(\xi R_B)K_1(\xi R_P))$

$\quad + \alpha\beta\phi(I_0(\xi R_B)K_0(\xi R_P)$

$\quad - K_0(\xi R_B)I_0(\xi R_P))\Big)$

$$A_5 = \left(P_g\phi\left(\sqrt{Da}R_P - 2\beta Da\right)\left(\xi\sqrt{Da}K_1(\xi R_B)\right.\right.$$
$$\left.+\alpha K_0(\xi R_B)\right)\big)/2\Big(\big(\xi\sqrt{Da}K_1(\xi R_P)$$
$$+\beta\phi K_0(\xi R_P)\big)$$
$$\left(\xi\sqrt{Da}I_1(\xi R_B) - \alpha I_0(\xi R_B)\right)$$
$$+\left(\xi\sqrt{Da}K_1(\xi R_B)\right.$$
$$\left.+\alpha K_0(\xi R_B)\right)\left(\beta\phi I_0(\xi R_P) - \xi\sqrt{Da}I_1(\xi R_P)\right)\Big)$$

$$A_6 = P_g\phi\left(2\beta Da - \sqrt{Da}R_P\right)\left(\alpha I_0(\xi R_B)\right.$$
$$\left.-\xi\sqrt{Da}I_1(\xi R_B)\right)/2\Big(\beta\xi\phi\sqrt{Da}I_1(\xi R_B)K_0(\xi R_P)$$
$$-\alpha\xi\sqrt{Da}K_0(\xi R_B)I_1(\xi R_P) - \alpha\xi\sqrt{Da}I_0(\xi R_B)K_1(\xi R_P)$$
$$+\beta\xi\phi\sqrt{Da}K_1(\xi R_B)I_0(\xi R_P)$$
$$+\xi^2 Da(I_1(\xi R_B)K_1(\xi R_P) - K_1(\xi R_B)I_1(\xi R_P))$$
$$+\alpha\beta\phi(K_0(\xi R_B)I_0(\xi R_P) - I_0(\xi R_B)K_0(\xi R_P))\Big)$$

where $\Delta = \sqrt{\theta_1^2 + 2\theta_2(P_g R_C - 2\tau_0)}$.

References

1. Akbar NS, Nadeem S, Mekheimer KS (2016) Rheological properties of Reiner–Rivlin fluid model for blood flow through tapered artery with stenosis. J Egypt Math Soc 24(1):138–142
2. Ashrafizaadeh M, Bakhshaei H (2009) A comparison of non-Newtonian models for lattice Boltzmann blood flow simulations. Comput Math Appl 58(5):1045–1054
3. Bali R, Gupta N (2018) Study of non-Newtonian fluid by K–L model through a non-symmetrical stenosed narrow artery. Appl Math Comput 320:358–370
4. Beavers GS, Joseph DD (1967) Boundary conditions at a naturally permeable wall. J Fluid Mech 30(1):197–207
5. Boodoo C, Bhatt B, Comissiong D (2013) Two-phase fluid flow in a porous tube: a model for blood flow in capillaries. Rheol Acta 52(6):579–588
6. Boyd W (1961) Text-book of pathology; structure and function in diseases. Lea and Febiger, Philadelphia
7. Bugliarello G, Sevilla J (1970) Velocity distribution and other characteristics of steady and pulsatile blood flow in fine glass tubes. Biorheology 7(2):85–107
8. Caro C (1982) Arterial fluid mechanics and atherogenesis. Clin Hemorheol Microcirc 2(1–2):131–136
9. Charm S, Kurland G (1965) Viscometry of human blood for shear rates of 0–100,000 sec-1. Nature 206(4984):617
10. Cokelet G (1972) The rheology of human blood. In: Biomechanics. Prentice-Hall, Englewood Cliffs, New Jersey
11. Elnaqeeb T, Mekheimer KS, Alghamdi F (2016) Cu-blood flow model through a catheterized mild stenotic artery with a thrombosis. Math Biosci 282:135–146
12. Goharzadeh A, Saidi A, Wang D, Merzkirc W, Khalil A (2006) An experimental investigation of the brinkman layer thickness at a fluid–porous interface. In: IUTAM symposium on one hundred years of boundary layer research. Springer, pp 445–454
13. Haldar K, Andersson H (1996) Two-layered model of blood flow through stenosed arteries. Acta Mech 117(1–4):221–228
14. Hill AA, Straughan B (2008) Poiseuille flow in a fluid overlying a porous medium. J Fluid Mech 603:137–149
15. Lih MMS et al (1975) Transport phenomena in medicine and biology. Wiley, Hoboken
16. Luo X, Kuang Z (1992) A study on the constitutive equation of blood. J Biomech 25(8):929–934
17. MacDonald D (1979) On steady flow through modelled vascular stenoses. J Biomech 12(1):13–20
18. Mekheimer KS, El Kot M (2015) Suspension model for blood flow through catheterized curved artery with time-variant overlapping stenosis. Eng Sci Technol Int J 18(3):452–462
19. Mekheimer KS, Zaher A, Abdellateef A (2019) Entropy hemo-dynamics particle-fluid suspension model through eccentric catheterization for time-variant stenotic arterial wall: Catheter injection. Int J Geom Methods Mod Phys 16(11):1950164
20. Misra J, Sinha A, Shit G (2008) Theoretical analysis of blood flow through an arterial segment having multiple stenoses. J Mech Med Biol 8(02):265–279
21. Ochoa-Tapia JA, Whitaker S (1995) Momentum transfer at the boundary between a porous medium and a homogeneous fluid-I. Theoretical development. Int J Heat Mass Transf 38(14):2635–2646
22. Ponalagusamy R (1986) Blood flow through stenosed tube. Ph.D. thesis, IIT Bombay, India
23. Ponalagusamy R, Tamilselvi R (2011) A study on two-layered model (Casson–Newtonian) for blood flow through an arterial stenosis: axially variable slip velocity at the wall. J Franklin Inst 348(9):2308–2321
24. Sharma BD, Yadav PK (2017) A two-layer mathematical model of blood flow in porous constricted blood vessels. Transp Porous Media 120(1):239–254
25. Srivastava V, Mishra S, Rastogi R (2010) Non-Newtonian arterial blood flow through an overlapping stenosis. Appl Appl Math 5(1):225–238
26. Sriyab S (2014) Mathematical analysis of non-Newtonian blood flow in stenosis narrow arteries. Computational and mathematical methods in medicine 2014
27. Straughan B (2008) Stability and wave motion in porous media. Springer, Berlin
28. Venkatesan J, Sankar D, Hemalatha K, Yatim Y (2013) Mathematical analysis of Casson fluid model for blood rheology in stenosed narrow arteries. J Appl Math
29. Whitaker S (1986) Flow in porous media I: a theoretical derivation of Darcy's law. Transp Porous Media 1(1):3–25
30. Whitmore RL (1968) Rheology of the Circulation. Pergamon, Bergama
31. Young D (1968) Effect of a time-dependent stenosis on flow through a tube. J Eng Ind 90(2):248–254
32. Zhang JB, Kuang ZB (2000) Study on blood constitutive parameters in different blood constitutive equations. J Biomech 33(3):355–360